Bioactive Silica-Based Coating on Stainless Steel Implants

121

Josefina Ballarre and Silvia M. Ceré

Contents

J. Ballarre (✉) · S. M. Ceré (✉)
Materials Science and Technology Research Institute (INTEMA), University of Mar del Plata – National Research and Technology Council (CONICET), Mar del Plata, Argentina
e-mail: jballarre@fi.mdp.edu.ar; smcere@gxmail.com

L. Klein et al. (eds.), *Handbook of Sol-Gel Science and Technology*,
https://doi.org/10.1007/978-3-319-32101-1_140

Abstract

In the field of body implants, surface plays an important role in the response of the tissue to the presence of foreign material. Surface modification by the application of coatings can be tailored to offer the best performance in service at the lowest cost. Coatings can improve the corrosion resistance limiting the diffusion of metal ions and products of corrosion in the body, along with enhancing the bioactivity of biocompatible metals by generating a natural union with the bone. The bioactivity can be achieved by adding bioactive particles to the coating than can react promoting new bone growth around the implant favoring its union with bone and muscle systems.

In this chapter, the performance of silica based sol-gel coatings with the addition of different bioactive particles (hydroxyapatite, wollastonite, glass, or glass ceramic) applied onto stainless steel AISI316L is analyzed in terms of in vitro analysis (surface, electrochemical, and bioactivity) and preliminary studies about in vivo behavior.

Introduction

Biomedical prosthesis devices are used for replacing a body part that is missing or has loosen functionality. Metallic materials are most commonly used for load bearing implants and internal fixation devices (Chen and Thouas 2015). Some featured properties of a metallic material are its high tensile strength, high yield strength, resistance to cyclic loading (fatigue), resistance to time dependent deformation (creep), and its corrosion resistance. They generally find applications in the fabrication of implant devices such as hip joint prosthesis, knee joint prosthesis, dental implants, cardiovascular devices, etc. The most commonly used metals and alloys for medical devices include stainless steels (AISI 316L/317L, ASTM F138), commercially pure titanium and its alloys and cobalt-based alloys and, to a lesser extent, tantalum, zirconium, and noble metals such as platinum and gold. It is important that their degradation by wear and/or corrosion is negligible (Duran et al. 2004). The metals used as permanent intracorporeal implants require the formation of a passive oxide film to prevent oxidation. The oxide is spontaneously formed on the metallic surface and limits the transport of metal ions across the oxide-solution interface. The passive film should be nonporous and fully cover the metal surface and also remain on the surface under mechanical stresses. The lower the amount of atomic defects in the oxide film, the more effective is the protection (Jacobs et al. 1999). The oxide formed on stainless steel alloys is susceptible to suffer localized corrosion in the body environment. Protective biocompatible coatings applied onto the alloys can delay the rejection on harmful ions to the surrounding hence improving the corrosion resistance of the stainless steel in body fluid (Hansen 2008).

Cemented and cementless prosthesis are used in orthopedic surgery and vast discussion about advantages and drawbacks of one procedure over the other are

claimed based on their relative cost, surgery procedure, and postoperative quality of life among others (Pennington et al. 2013). Cementless prosthesis are generally preferred for young active patients since there is more bone conservation, less probability of loosening and also, for patients who are allergic to methylmethacrylate. A study presented on cementless primary total hip arthroplasty shows satisfactory results in the short time and tend to improve in time, being promising in the case of a revision surgery (Rothman and Cohn 1990). The surface of the prosthetic metallic devices can be modified in order to promote bioactivity and hence not require the use of cement to attain fixation to the host. Coatings can be formulated with that goal and applied onto the metal to be bioactive and promote cell proliferation and osseointegration (Goriainov et al. 2014).

In this chapter, the performance of silica based sol-gel coatings with the addition of different bioactive particles (hydroxyapatite, wollastonite, glass, or glass ceramic) applied onto stainless steel AISI316L is analyzed in terms of in vitro analysis (surface, electrochemical, and bioactivity) and preliminary studies about in vivo behavior.

Stainless Steel Implants

Stainless steels (SS) are iron-base alloys with a minimum of 10.5% Cr as an alloying element, needed to form a passive film of chromium oxide on the surface. Stainless steel (18Cr–8Ni) was first used in orthopedic surgery in 1926 (Helsen and Breme 1998). Special production techniques such as vacuum melting, vacuum arc melting, and electro slag refining are required to produce high-quality stainless steels with minimum nonmetal inclusions for implant applications. Besides, the use of SS for implant applications, commercial-grade stainless steel is also widely used for the manufacture of surgical and dental instruments.

Among the different types of stainless steels, AISI 316L stainless steel is the more commonly employed for temporary devices such as fracture plates, bone screws, and hip nails due to its low cost and acceptable biocompatibility (Biehl and Breme 2001; Okazaki and Gotoh 2005). It is worth noting that, in developing countries, SS is also employed as permanent implants. Surgical grade AISI316L implants corrode in the human body environment and release Fe, Cr, and Ni ions. These ions can act as allergens and carcinogens. Studies developed on retrieved stainless steel implants show that more than 90% of the failure associated with the material are due to pitting and crevice corrosion attack (Hansen 2008). That is why for permanent prosthetic stainless steel components there is a need of protection of the metal oxide surface in the body environment. One way to minimize the release of corrosion products from the implant to the surrounding tissue is to apply protective coatings: sol-gel method has been proposed as a suitable procedure to generate protective (Balamurugan et al. 2006; Ballarre et al. 2007b; de Damborenea et al. 1995; de Sanctis et al. 1990; Galliano et al. 1998) and bioactive coatings (Ballarre et al. 2012; Gallardo et al. 2001) when bioactivation is a goal to be achieved for cementless devices.

Stainless Steel's Degradation: Corrosion and Wear

Corrosion

The in situ degradation of a metal implant is an undesirable phenomenon for two main reasons: the degradation process can lose the structural integrity of the implant and the release of corrosion products can cause adverse biological reaction in the host. Degradation phenomena may be generated by electrochemical dissolution, wear, or a synergistic combination of both. Electrochemical processes may include generalized corrosion, affecting uniformly the implant surface and localized corrosion affecting some regions of the device due to geometric factors (crevice corrosion) or at random points of the surface (pitting corrosion). Electrochemical and mechanical processes can also interact, causing premature failure and accelerating the release of metal particles or ions.

Corrosion in orthopedic materials is a complex multifactorial phenomenon that depends on the geometry, metallurgical parameters, and mechanical and chemical solution. So, any advance in the comprehension of these factors and their interactions is required to understand why the implants corrode and how to prevent it.

Wear

One of the major requirements for satisfactory performance long-time mobile orthopedic prostheses is their ability to work and function without damage under any conditions of motion. Because damage is caused by various stresses, the material of each component of the prosthesis (in total hip replacement prosthesis for example) must show high wear resistance due to sliding induced friction or rubbing, low friction coefficient to minimize compressive stresses; and the modulus of elasticity must be less or equal to the bone, in order to efficiently absorb the stresses on the stem and only transmit small loads to the acetabulum. To simulate the multiple stresses to which the different parts of a total hip replacement are subject quite complex modeling and experimental systems are required. Preliminary analysis of the forces of friction and wear phenomena can begin by testing simpler and standardized wear. This is why the measurement of coefficient of friction (COF) and the adhesion force and the analysis of the events and mechanisms that take place during scratch are important key issues to simulate wear in thin films applied onto surgical grade stainless steel.

Another extremely important parameter for the smooth functioning of replacement parts is the surface roughness of almost every piece. In the case of a total hip implant, the stem and the outer face of the acetabulum cup is desirable to have controlled roughness to promote adherence of progenitor cells and facilitate bone osseoconduction (Cacciafesta et al. 2001; Harris and Beevers 1999; Martin et al. 1995). Good lubrication and low surface roughness are two required conditions

to prevent the release of wear particles that can then remain in the surrounding tissues causing injuries, high concentration of potentially harmful ions, and estrange body phenomenon (Doorn et al. 1998; Kempf and Semlitsch 1990; Kim et al. 2001; McGee et al. 2000; Semlitsch and Willert 1997; Sychterz et al. 2000; Willert and Buchhorn 1993).

Protection Against Degradation: Silica Based Thin Films

As it was stead above, wear and corrosion of the metallic implant can lead to the release of metallic particles causing different pathologies that could finally end in the removal of the implant. One of the ways to improve the ion release from the alloy is to apply a coating onto the metallic implant that acts as a protective layer. Among the coatings used to improve the performance of metallic prosthesis, the silica based type with silane precursors showed biocompatibility (Peterson et al. 2005) and good adherence to the substrate. Nevertheless, the main disadvantage of glassy coatings is their fragility. Hybrid organic–inorganic films with high content of silica can overcome this drawback being an alternative to improve the mechanical properties of vitreous coatings since the addition of some organic groups is expected to give plastic characteristics to the films while preserving the property of being a protective and dense net. Inorganic–organic hybrid sol-gel materials are interpenetrating networks of inorganic and organic components that interact at the nanoscale (Novak 1993). The two components are indistinguishable above the nanoscale. This is different from nanocomposites, which have distinguishable components. However, synthesis of hybrids is complex and there are several chemistry challenges that must be overcome before hybrids can be successfully used in tissue regeneration. Hybrids are synthesized introducing the polymer early in the sol-gel process, e.g., after hydrolysis of tetraethoxysilane (TEOS) – a basic alkoxide of silicon oxide network precursor, so that the inorganic (silica) network forms around the polymer molecules, resulting in molecular-level interactions (Brinker and Scherer 1990). The thermal processing has to be modified from conventional sol-gel glass synthesis. Most hybrid systems are aged and dried below 100 °C. The hypothesis is that the fine-scale interactions between the organic and inorganic chains lead to a material that behaves as a single phase, resulting in an increase of the intra-connectivity of the inorganic domains, modify the inorganic network structure (degree of branching, crosslink density, etc.), and the potential for tailoring the mechanical properties (Novak 1993).

Hybrid thin films can provide the material the capability of being a protective bio-inert connector between the metallic prosthesis and the bone tissue. Also, superficial features as toughness, friction coefficient, and adhesion of the coating to the substrate are of great importance for a complete mechanical characterization. The orthopedic prosthesis are inserted in the human body through a surgical procedure that involves high stresses; therefore, the mechanical, adhesive, and wear

behavior of their surfaces is a very important issue from the very beginning of the implantation life of the component to be placed in the body.

Tetraethoxysilane Based Coatings

The use of silica based coatings produced by hydrolysis and polycondensation of tetraethoxysilane (TEOS) and other derived alcoxides is widely used as protection against scratching and for antireflex coatings in glasses (Duran et al. 1986). The uses of this kind of coatings applied onto metals started in the 1990s with the aim of improving the corrosion resistance of aluminum alloys. The so-called hybrid organic–inorganic coatings, not only made by Si-O bonds, but containing some organic ligands, generate a more plastic coating that could adapt better to different geometry and roughness of the substrate (Guglielmi and Zenezini 1990; Innocenzi et al. 1992).

TEOS-MTES Coatings

The combination of tetraethoxysilane (TEOS) and methyltriethoxysilane (MTES) applied onto surgical grade stainless steel has been studied as a basic coating for corrosion protection and a possible holder for bioactive or functional particles (Ballarre et al. 2007b; Galliano et al. 1998, 2001). This type of coating has been evaluated superficially, mechanically, and electrochemically, as is going to be described ahead.

TEOS-MTES + SiO_2 Nanoparticles

The addition of nano-colloidal silica to the TEOS-MTES solution could reinforce the structure of the films and enhance its protective behavior to the aggressive body fluids. Hybrid organic–inorganic sols with these particles can be prepared like typical TEOS-MTES sols and a water based solution with colloidal silica (Ballarre et al. 2009a, c). The new hybrid reinforced coatings (TEOS-MTES-SiO_2) are formulated by adding different amount of silica nanoparticles in order to offer an improved corrosion resistance to the substrate. The average thickness obtained (profilometer KLA Tencor, Alpha-Step D-100, US) resulted 2.1 $\pm$ 0.2 (for 10% of SiO_2) and 2.3 $\pm$ 0.2 μm (for 30% of SiO_2) higher than the value of 1.5 $\pm$ 0.2 μm obtained for TEOS-MTES coating without SiO_2 nanoparticles. Figure 1 shows the scanning electron microscopy (SEM) images of the transversal cut of the TEOS-MTES with 10% in weight of SiO_2 nanoparticles coating, where the thickness of the film can be observed together with the continuity of the coating on the substrate.

TEOS- γ-MPS and TMH Coatings

Other type of hybrid coating, with a more organic content, is the one made from the hydrolysis and polycondensation of TEOS, 3-methacrylopropyl trimethoxysilane) (γ-MPS), and hydroxyethyl metacrilate (HEMA). These coatings have large

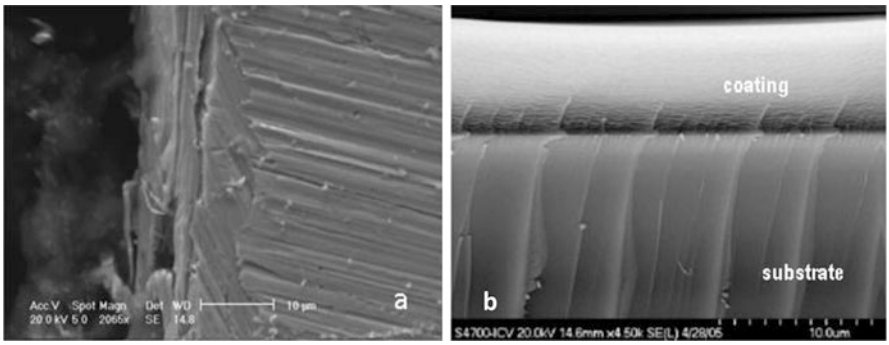

Fig. 1 Scanning electron microscopy (*SEM*) of the silica based TEOS-MTES-SiO_2 10% coatings. (**a**) Image denoting the adherence of the coating to the AISI316L steel; (**b**) detail of thickness of a double layer

thickness and a more open structure than the previous ones (Ballarre et al. 2008b; López et al. 2008b). The new organic inorganic coating is called by the authors as TMH and it was studied regarding its adherence to the substrate, mechanical properties, and corrosion resistance. Two kinds of coatings are presented for the study: a single layer of TMH with a thickness of 3.5 μm and a double layer of TEOS-MTES/TMH of 3.8 μm thickness.

In all these types of coatings, the thermal treatment is another point to take into account since it can either consolidate or degrade the thin film. Also the temperatures and time under the heat treatment could affect the mechanical surface characteristics of the metal, in this case the stainless steel AISI 316L. Temperature above 750 °C and heat treatments above 8 h can induce sensitization and changes in the metallic structure (and thus its corrosion resistance) of this kind of stainless steel (Kashyap et al. 1988).

In Vitro Analysis for TEOS-MTES, TMH, and TEOS-MTES-$SiO_{2\ nano}$ Coatings on Stainless Steel Substrates

The coated systems are analyzed in vitro by immersion in a solution that simulates the inorganic concentration of ions in the human plasma at 37 °C. The objective is to detect presence of hydroxyapatite, analyze the degradation of the coating, and to simulate long exposition to corrosive fluids. One of the most used inorganic simulated body fluid (SBF) solution is the one proposed by Kokubo et al. SBF is prepared with the following chemical composition (Kokubo et al. 1990): NaCl (8.053 g./L), KCl (0.224 g/L), CaCl2 (0.278 g/L), $MgCl_2.6H_2O$ (0.305 g/L), K_2HPO_4 (0.174 g/L), $NaHCO_3$ (0.353 g/L), $(CH_2OH)_3\ CNH_2$ (6.057 g/L). Concentrated hydrochloric acid (HCl) is added to adjust the pH to 7.25 ± 0.05.

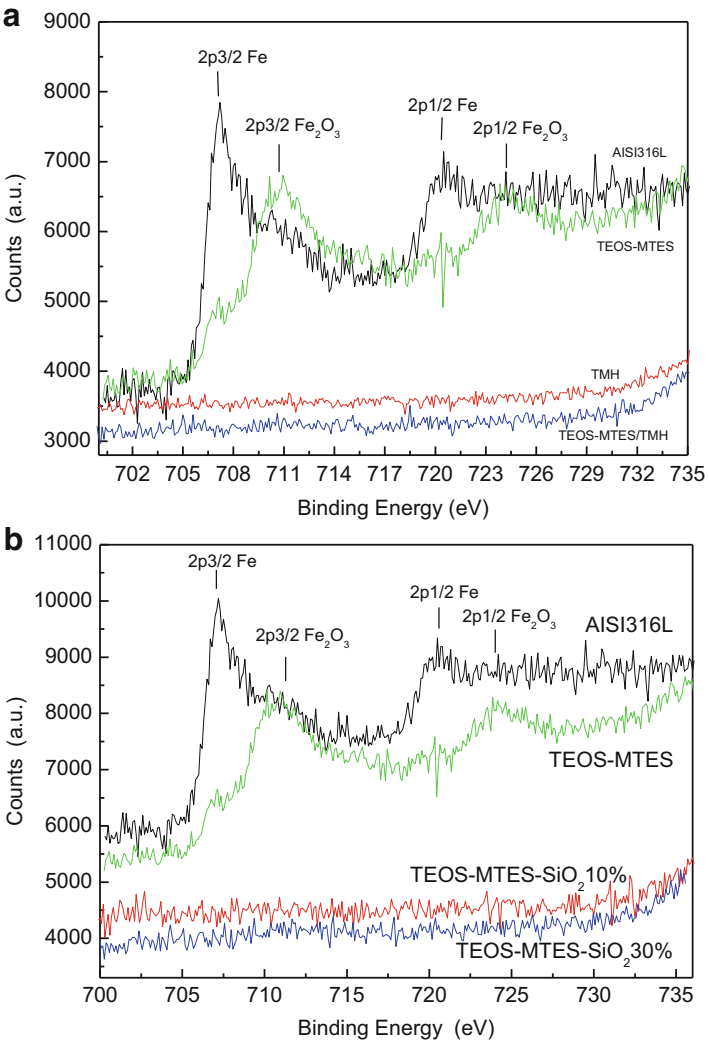

Fig. 2 X-ray photoelectron spectroscopy (*XPS*) high resolution spectra for Fe 2p region with 120 s of Ar^+ exposition for (**a**) the bare stainless steel AISI316L, stainless steel with TEOS-MTES, TMH, and TEOS-MTES/TMH coatings, after 30 days immersion in simulated body fluid (*SBF*); (**b**) the bare stainless steel AISI316L, stainless steel with TEOS-MTES, TEOS-MTES with 10% and 30% silica nanoparticles, after 30 days immersion in simulated body fluid (*SBF*)

Surface characterization of the coated systems can be performed by a broad variety of techniques; among them the most used are SEM, X ray photoelectron spectroscopy (XPS), X ray diffraction (XRD), and Raman spectroscopy

Figure 2 presents the high resolution XPS scans for Fe 2p with 120 s of sputtering with Ar^+ in the coatings after immersion in SBF for 30 days for coated AISI 316L

with TEOS-MTES, TMH, and double layers combining TEOS-MTES + TMH as top coating. It can be observed that Fe is only detected in the TEOS-MTES hybrid coating, not showing Fe signal in the samples coated with TMH or double-layer coatings. The bigger thickness of these coatings compared with the TEOS-MTES ones limits the Fe diffusion to the surface, demonstrating the barrier effect of the coatings against ion diffusion.

Mechanical and Wear Properties of TEOS-MTES, TMH, and TEOS-MTES-SiO_2 Nano Coatings on Stainless Steel AISI 316L Substrates

One of the main drawbacks of glass coatings is their brittleness. As it was already said above, the hybrid organic–inorganic films with high content of silica are presented as an alternative to improve the mechanical properties of vitreous coatings preserving their protectiveness and high density of the films (Amato et al. 2005; Ballarre et al. 2002). Besides, it is possible to obtain thicker films when increasing the proportion of organic compounds in the sol-gel process. Also, superficial features as the roughness or friction coefficient and the adhesion of the coating to the substrate are of great importance for a complete mechanical characterization. As the implanting procedure is performed by applying high tension and loads on the prosthesis during the surgery, it is important to evaluate the mechanical, adhesive, and wear properties of the implant surface in order to avoid future failure of the materials. There is no much information about the friction coefficient or the adhesion of silica based hybrid organic–inorganic coatings on stainless steel. One of the most recent techniques used to study the mechanical properties of thin films is the instrumented indentation, known as nanoindentation. This is a surface technique to measure quasi-statically the penetration of an indenter at increasing loads applied to a material. With a modulus of lateral force, and a ramped load in a displacement (scratch) path, the nano-scratching test is implemented (Li-Ye Huang et al. 2002; Li et al. 2005; Scharf and Barnard 1997; Simunkova et al. 2003; Guohua Wei et al. 2004). Young's modulus and hardness of hybrid coatings on stainless steel substrates were recently analyzed (Ballarre et al. 2007a) and mechanical properties of similar films have been also studied (Malzbender et al. 2000; Prikryl et al. 2005; Soloukhin et al. 2002). Both the Young's modulus and the hardness and other relevant data of the silica based films are analyzed from the load-displacement curves (Ballarre et al. 2008a; Oliver and Pharr 1992) of the nanoindentation experiments. The analysis of indentation load-penetration curves produced by instrumented indentation systems is often based on the work developed by Oliver and Pharr (Oliver and Pharr 2004) and based upon relationships established by Sneddon (Sneddon 1965). The results are analyzed according to the eq.:

$$S = 2aE_r = \frac{2\beta}{\sqrt{\pi}} E_r \sqrt{A}, \tag{1}$$

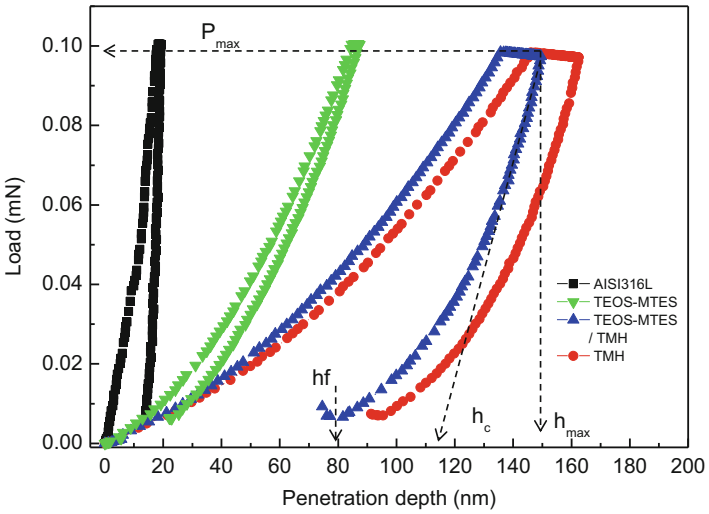

Fig. 3 Load-unloading versus displacement curves for the TEOS-MTES, TMH, and TEOS-MTES/TMH coatings tested with a maximum load of 0.1 mN. The typical AISI316L stainless steel behavior is also shown (From Ballarre et al. (2008a))

where a is the contact radius and A is the projected area of the tip sample contact. β is used to account for the triangular and square cross-sections of many indenters used in nanoindentation studies. The values of β for different indenters were determined by King (King 1987) and other authors (Dao et al. 2001). For a Berkovich indenter, $\beta = 1.096$ (Fischer-Cripps 2006).

The stiffness (S) is determined as the slope S = dP/dh of the upper portion of the unloading curve, where P is the applied load and h is the displacement. Figure 3 shows a graph of load versus indenter displacement data for an indentation test where hmax is the maximum displacement at maximum applied load (Pmax) and h_f is the final depth of the contact impression after unloading. Er is the reduced modulus defined by the eq.:

$$\frac{1}{E_r} = \frac{(1-\nu^2)}{E} + \frac{(1-\nu_i^2)}{E_i}, \tag{2}$$

where E and ν are the Young's modulus and Poisson's ratio of the specimen, and E_i and ν_i are the modulus and Poisson's ratio for the indenter ($E_i = 1140$ GPa and $\nu_i = 0.07$ for a diamond Berkovich type indenter). For all samples shown in the Figs. 3, 4, 5, 6, 7, and 8 a Poisson's ratio equal to 0.25 was used.

The hardness was determined using the eq.:

$$H = \frac{P_{\max}}{A_c}, \tag{3}$$

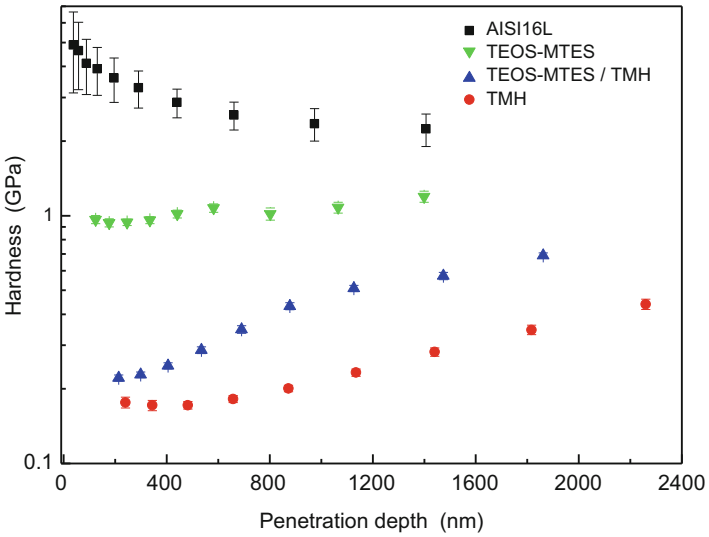

Fig. 4 Young's modulus profiles of TEOS-MTES, TEOS-MTES/TMH, TMH coatings, and the AISI 316L stainless steel substrate (From Ballarre et al. (2008a))

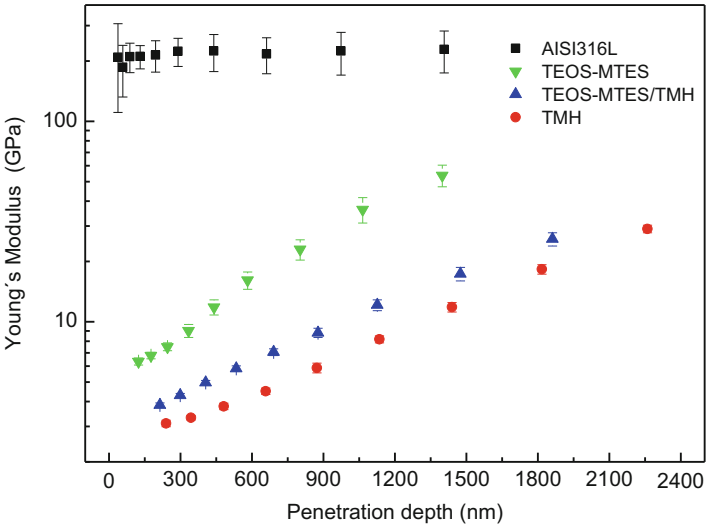

Fig. 5 Hardness profiles of TEOS-MTES, TEOS-MTES/TMH, TMH coatings, and the AISI 316L stainless steel substrate (From Ballarre et al. (2008a))

where A_c is the area of the indentation at a maximum applied load, P_{max}. By precisely knowing the geometry of the indenter (by calibration), A_c can be expressed in terms of the contact depth (hc) directly determined from the measurements.

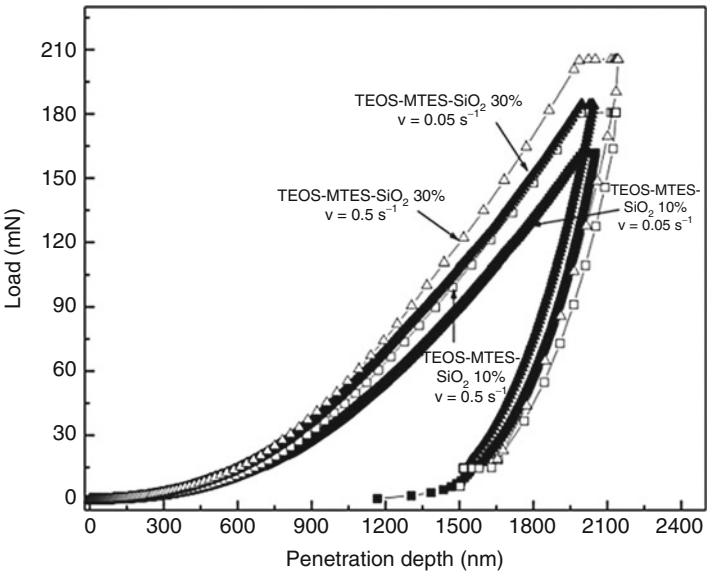

Fig. 6 Load–displacement curves for the TEOS-MTES-SiO_2 coatings with 10% of silica nanoparticles and a deformation rate of 0.05 s^{-1} (■) and 0.5 s^{-1} (□); and for TEOS-MTES-SiO_2 coatings with 30% of SiO_2 and a deformation rate of 0.05 s^{-1} (▲) and 0.5 s^{-1} (Δ) (From Ballarre et al. (2009a))

The results for the nanoindentation data for the TEOS-MTES, TMH, and a combination of both coatings (TEOS-MTES/TMH) as well as for the substrate for a maximum applied load of 0.1 mN are presented in Fig. 3. In this figure, the values of Pmax, hc, hmax, and hf extracted from the experimental data for the TEOS-MTES/TMH are shown as an example. When the Pmax (0.1 mN) was applied, the highest final penetration hf (93 nm) was obtained for the TMH coating in which the organic concentration was higher than in the TEOS-MTES coatings. The lowest final penetration (21 nm) corresponded to the TEOS-MTES coating, similar to the value of the substrate (13 nm). The TEOS-MTES/TMH presented an intermediate value of penetration (81 nm). These hf values indicate a decrease in the plastic character of the coatings in the order TMH > TEOS-MTES/TMH > TEOS-MTES. Typical curve for the metallic substrate is shown as comparative data. The use of sharp indenters, as Berkovich, induces very high stress for low loads as compared to other type of indenters (Wolf 2000). The plastic zone, especially in metals, is very small and is difficult to recognize with optical or SEM images. In this case, it was assumed that the offset of plasticity is only reached at high loads because of the non-superposition of the loading and unloading curve.

By comparing the indentation data of the three types of coatings and the data from the substrate, both the Young's modulus (E) and the hardness (H) as a function of depth penetration can be obtained using the Oliver and Pharr model and the corrections for the upper fraction of the curve (Figs. 4 and 5, respectively). In the

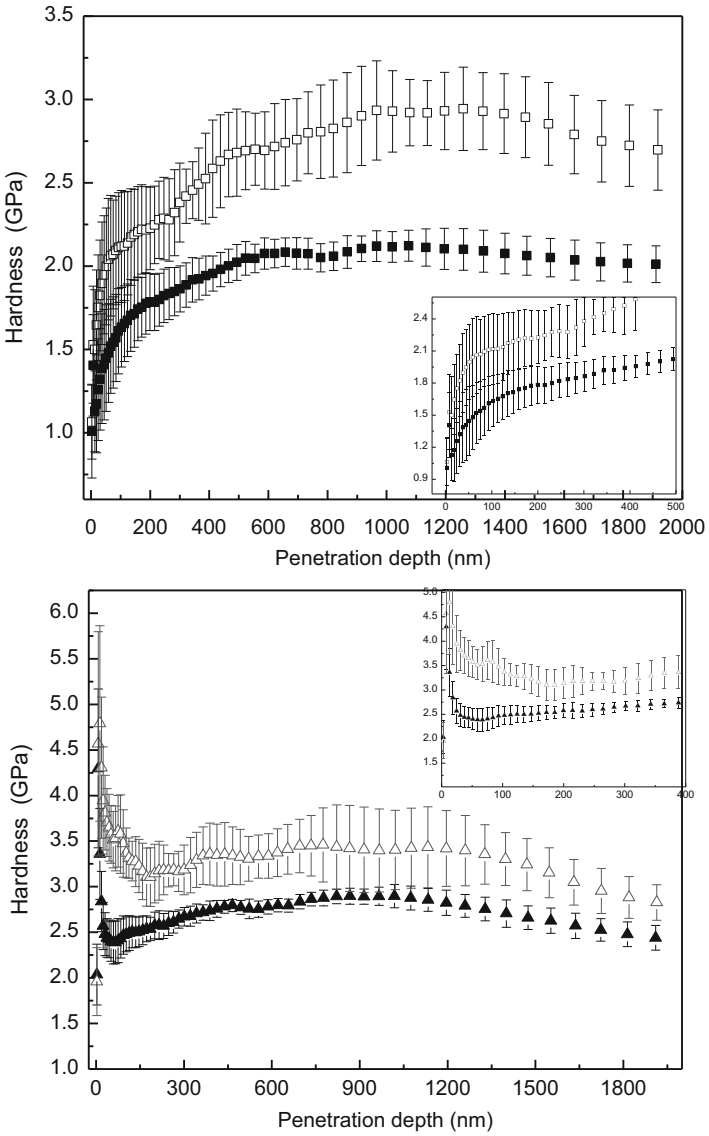

Fig. 7 Hardness (H) vs. depth penetration into the coating thickness for: (**a**) the TEOS-MTES-SiO_2 10% with strain rate of 0.05 s^{-1} (■) and 0.5 s^{-1} (□), and for (**b**) TEOS-MTES-SiO_2 30% coating with strain rate 0.05 s^{-1} (▲) and 0.5 s^{-1} (Δ) (From Ballarre et al. (2009a))

data presented it was assumed that the values are not influenced by the substrate (Lucas et al. 1998). A large number of models and methods can be used to deduce some mechanical properties of the coated materials, and there are many interesting papers published about that (Atanacio et al. 2005; Chicot and Lesage 1995; Jönsson

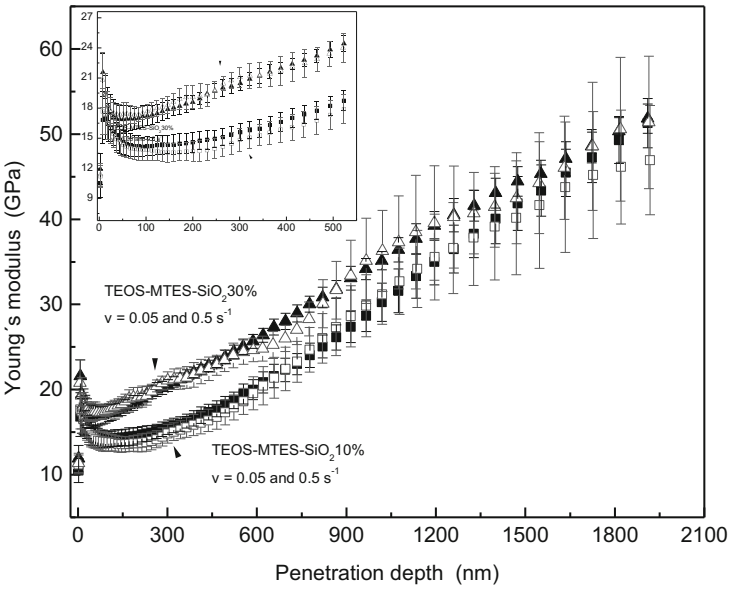

Fig. 8 Young's modulus (E) vs. depth penetration into the coating thickness for the TEOS-MTES-SiO_2 10% with strain rate of 0.05 s^{-1} (■) and 0.5 s^{-1} (□), and for TEOS-MTES-SiO_2 30% coating with strain rate 0.05 s^{-1} (▲) and 0.5 s^{-1} (Δ) (From Ballarre et al. (2009a))

and Hogmark 1984; Karimi et al. 2002; Lesage et al. 2004; Li et al. 2005; Mammeri et al. 2006; Nakonechna et al. 2004; Wei et al. 2004). Ballarre et al. presented Young's modulus and hardness of hybrid coatings evaluating the depth profile data at 10% of the film thickness (Ballarre et al. 2008a). It is worth noting that this 10% rule of thumb does not take into account neither the particular properties of the hard substrate and the soft film used nor the deformation mechanisms involved during the indentation. The unflawed state is quite important for biomedical applications in order to avoid corrosion or wear events. In all of the samples analyzed no film cracking was observed after indentation. However, it has to be considered that low loads were applied.

A remarkable rise in the Young's modulus values with the increase of penetration depth is observed in Fig. 4. A similar dependence can be observed with the hardness for the TMH and TEOS-MTES/TMH coatings in Fig. 5. This behavior could be attributed to the influence of the elastic characteristics of the substrate. The coating with the highest amount of organic components (TMH) showed the lower superficial modulus and hardness. This fact was attributed to the increase of polymeric network formed induced by the 2-hydroxyethyl methacrylate (HEMA). The most vitreous coating (TEOS-MTES) showed the highest elastic modulus and hardness. These values can be associated to the different degree of elasticity of the coatings as presented above.

When silica nanoparticles are added to the coatings, mechanical properties become an even more important issue, since they should reinforce the coatings together with an improvement in corrosion behavior.

As the incorporation of silica nanoparticles to the hybrid sol has as main objective to reinforce the structure of the films and enhance its corrosion resistance, the effect of the adding of nanoparticles to the TEOS MTES sol was studied by Ballarre et al. (2009a, c, Ballarre et al. 2010). Two kinds of TEOS-MTES coating with different amounts of silica nanoparticles (10% and 30% wt) are compared at two different deformation rates (0.05 and 0.5 s^{-1}). This change in the experimental setup parameter of the nanoindentation tests can be noticed in loading-unloading curves of the coatings (Fig. 6). The maximum applied load varies in each assay since the test is programmed for a given maximum penetration depth. Figure 6 shows that when the samples are slowly indented or deformed, the maximum applied load is smaller that when a bigger deformation rate is applied. The coatings made with TEOS-MTES and 30% wt. of silica nanoparticles presented the highest maximum load, and it could represent a major stiffness of these kinds of systems. This fact seems to be due to the amount of colloidal spherical nanoparticles, which have a larger elastic modulus than the matrix and could also be compacted during the nanoindentation process.

Figures 7a, b, and 8 represent the obtained values for the Young's modulus (E) and the hardness (H) versus the penetration depth for the analyzed samples (with 10% and 30% of colloidal silica nanoparticles), employing the continuous stiffness data. The values of the mechanical properties for the TEOS-MTES coating containing 10% wt. of silica nanoparticles are smaller than for the 30% wt. coating at the first part of the curve, where the influence of the substrate is lower (Lucas et al. 1998). The main value of the Young's modulus was taken at 200 nm depth penetration on the coating. Again, this improvement of stiffness is due to an increase of packing events of the nanoparticles in the reinforced coatings. A different effect is noticed in hardness measurements. The samples with major content of silica nanoparticles have again the higher values of H, but they seem to be affected by the rate of deformation (Fig. 7b), showing high values at faster deformation velocities (0.5 s^{-1}) due to visco-elastic effects.

The quasi-invariability of the elastic modulus values with the increment of the deformation rate could be explained with the unchanged composition of the TEOS-MTES coating matrix, where the organic and inorganic compounds ratio remained constant. Furthermore, other characteristics of the system that could alter the modulus, like temperature and crystallinity ('locked' segments) (Montemor et al. 2006), also remained constant showing almost no change of the Young modulus with strain rate.

A summary of the results of E and H values can be seen in Table 1.

To analyze the adherence and scratch resistance of the hybrid coating, other nanoindentation experiments can be done (Ballarre et al. 2009b). By applying a lateral force modulus, and a ramped load in a displacement path (scratch), a nano-

Table 1 Young's modulus (e) and hardness (h) values found for teos-mtes-sio$_2$ 10% and 30% coatings on aisi316l stainless steel (ss) with nanoindentation at deformation rate 0.05 s^{-1} (Ballarre et al. 2009a), and teos-mtes, tme, and teos-mtes/tmh coatings on the same substrate (Ballarre et al. 2008a)

	E (GPa)	H (GPa)
AISI 316L substrate (SS)	187 ± 18	2.3 ± 0.1
SS + TEOS-MTES coating	6.5	0.92
SS + TMH coating	3	0.16
SS + TEOS-MTES + TMH coating	3.8	0.22
SS + TEOS-MTES-SiO_2 10% coating	14 ± 3	1.8 ± 0.3
SS + TEOS-MTES-SiO_2 30% coating	16 ± 3	2.5 ± 0.3

scratching test can be done on the coated sample surface (L-Y. Huang et al. 2002; Li et al. 2005; Simunkova et al. 2003; Wei et al. 2004).

The film with high content of organic compounds (TMH) has elastic recovery until 75 mN of applied load. The coating suffers plastic deformation but not delamination. After the unloading, the film has a persistent deformation and is removed due to the asynchronic recovery of the film and the substrate. The TEOS-MTES/TMH coating shows a lot of debris in the trace. This is an unusual but possible behavior and could be attributed to different recovery between the substrate, the first TEOS-MTES layer and the upper TMH film. This fact produces delamination and crack formation in the TEOS-MTES coating, inducing tensile tensions, and finally the upper film is pulled-off. The film with highest inorganic content (TEOS-MTES) denotes the lowest friction coefficient. The TMH and the dual TEOS-MTES/TMH coatings have similar values, indicating that the lower inorganic layer does not affect the friction with low loads applied.

A more detailed analysis is made by comparing the beginning (up to applied normal load = 80 mN) of the pre-scan, scratching, and post-scan curves with the coefficient of friction (COF) curves (Fig. 9a–c for TEOS-MTES, TMH, and TEOS-MTES/TMH, respectively). The optical images of the three coatings are also shown (Fig. 9d–f). For the TEOS-MTES coating, it can be pointed that the film remains with a constant elasto-plastic deformation until 20 mN. At higher loads the tip of the indenter reaches the substrate (film thickness = 1.2 μm) and the failure of the coating by delamination is observed. Some fluctuations are observed in the COF after 25 mN because of the release of debris caused by the chipping process.

In the case of the TMH and the TEOS-MTES/TMH coatings, the thickness of the films (3.5 and 3.8 μm, respectively) are higher than the thickness of coating with only TEOS-MTES (2 μm), and hence the substrate is not reached in the range of loads analyzed. The initial behavior is similar in both materials, until a load of 15 mN. Elastic deformation is observed and it is associated with the indenter penetration in the coatings at low loads, as can be seen in the COF curve (Fig. 9b, c). The deformation continues in both cases, but there is a change in the TEOS-MTES/TMH

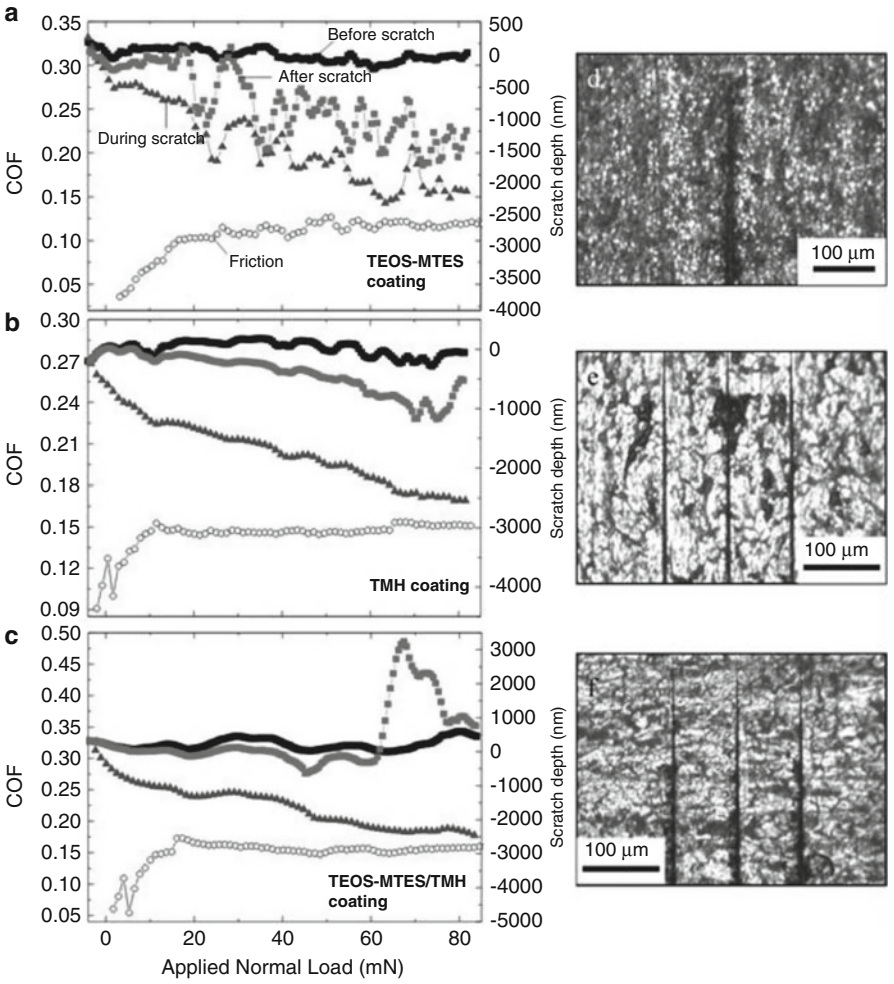

Fig. 9 Coefficient of friction (*COF*) and scratch depth profiles as a function of increasing normal load (**a**, **b,** and **c**) and optical images (**d**, **e,** and **f**) of the TEOS-MTES, TMH, and TEOS-MTES/TMH coatings on surgical grade stainless steel after nano-scratch experiment. The optical images were taken at the beginning of the scratch process (From Ballarre et al. (2009b))

system behavior, associated to the fracture of the inner and more inorganic coating (TEOS-MTES). The chipping of the coating that is caused by the formation of radial cracks is observed optically in the photograph beside the TEOS-MTES/TMH scratch curve (Fig. 9f). The film with highest inorganic content (TEOS-MTES) has almost no elastic response, but their debris or the material removed due to chipping or delamination does not persist into the indentation trace.

The nano-scratch technique is successfully used for mechanical characterization of hybrid organic–inorganic thin films. The adhesive behavior can be analyzed in order to distinguish deformation events, delamination, or plowing.

Corrosion Resistance for TEOS-MTES, TMH, and TEOS-MTES-SiO_2 Nano Coatings on Stainless Steel AISI316L Substrates

Is well known that the metals used in orthopedic surgery are conditioned by the physiological media where there are exposed and that could lead to the release of nondesired metallic particles or potentially harmful ions to the human body (Jacobs et al. 1999; Park 1984; Woodman et al. 1983). In several occasions, the presence of a high concentration of metallic ions in the surrounding tissues near the implant has been detected coming from wear events, electrochemical reactions, or a combination of both of them. The body response can vary from a passive tolerance to a severe reaction of the host, leading to a generalized hypersensibility with the implant movement and then loosening of the prosthesis (Steinemann 1996). All alloys used as possible permanent implants have a passive oxide layer that forms spontaneously over the surface. However, all the metallic implants corrode at some extent in vivo, releasing corrosion products. In developed countries, the use of AISI 316L stainless steel is mostly limited to temporary implants or fixation plates since its corrosion resistance in physiological fluids is limited compared with titanium or cobalt-chromium alloys. As stainless steel is susceptible to suffer localized corrosion in chloride media (López et al. 2008a), the application of a coating on the surface with the purpose of isolating the substrate from the body fluid is proposed to extend life service of stainless steel (Balamurugan et al. 2007; Ballarre et al. 2012; Duran et al. 2004). The protective layer system is often composed of a two layers coating, with complementary properties: one inner layer devoted mainly to the protection to the substrate and one top layer chemically coherent with the inner layer and that can be functionalized in order to bioactivate the surface for cementless devices. The inner layer is prepared using TEOS and MTES (containing or not nanoparticles of SiO_2 as reinforcement) that has already shown very low iron diffusion by XPS. The top layer usually acts as a container for the later aggregate of bioactive particles, as the following step to induce the formation of hydroxyapatite shortcoming the bioactive response.

Figure 10 shows the potentiodynamic polarization curve for the coatings obtained with the TEOS-MTES hybrid coating. It can be observed that TEOS-MTES coatings act as an effective barrier to the electrolyte entrance in the coating after 1 day of immersion in SBF showing less passivity current density and a shift of the breakdown potential (Ebreak) of 0.85 V respect to the bare alloy (Amato et al. 2005; Gallardo et al. 2001; Garcia et al. 2004). The breakdown potential is defined as the potential where the current density of the sample increases dramatically with the potential. After 30 days of immersion the film slightly deteriorates, but it always remains with less passive current density and higher Ebreak than the bare material.

Figure 11 shows the potentiodynamic polarization curve for the coating that combines both hybrid systems (TEOS-MTES and TMH). After 1d of immersion

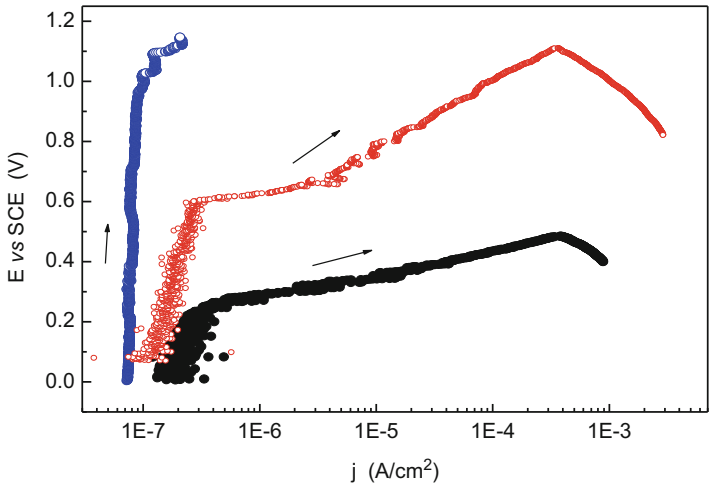

Fig. 10 Potentiodynamic polarization curve for the coatings obtained with the TEOS-MTES hybrid coating with (o) 1 day and (o) 30 days of immersion in SBF. Bare AISI316L (•) is shown for comparison. The *arrows* indicate the direction of polarization (From López et al. (2008b))

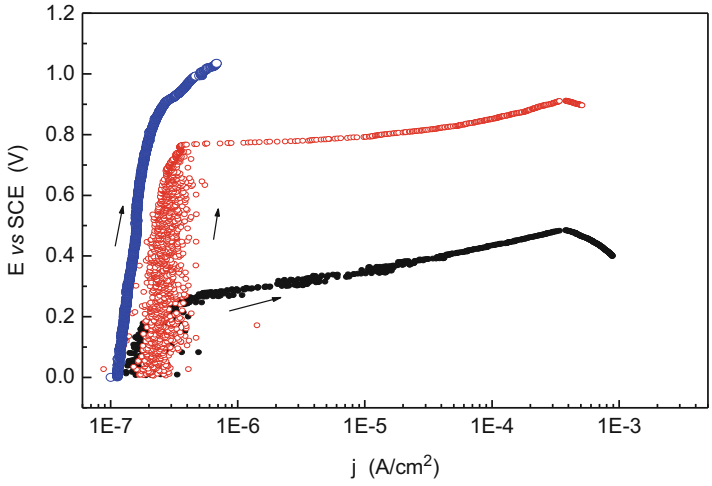

Fig. 11 Potentiodynamic polarization curve for the coating that combines both hybrid systems (TEOS-MTES/TMH), with (○) 1 day and (o) 30 days of immersion in SBF. Bare AISI316L (•) is shown for comparison. The *arrows* indicate the direction of polarization (From López et al. (2008b))

the performance is very similar to that presented for the TEOS-MTES system. After 30 d of immersion the current density around the corrosion potential is analogous to the other studied systems, but the E_{break} is shifted positive respect to both systems, reaching 0.8 V. The double-layer coating acts as a barrier to corrosion at the

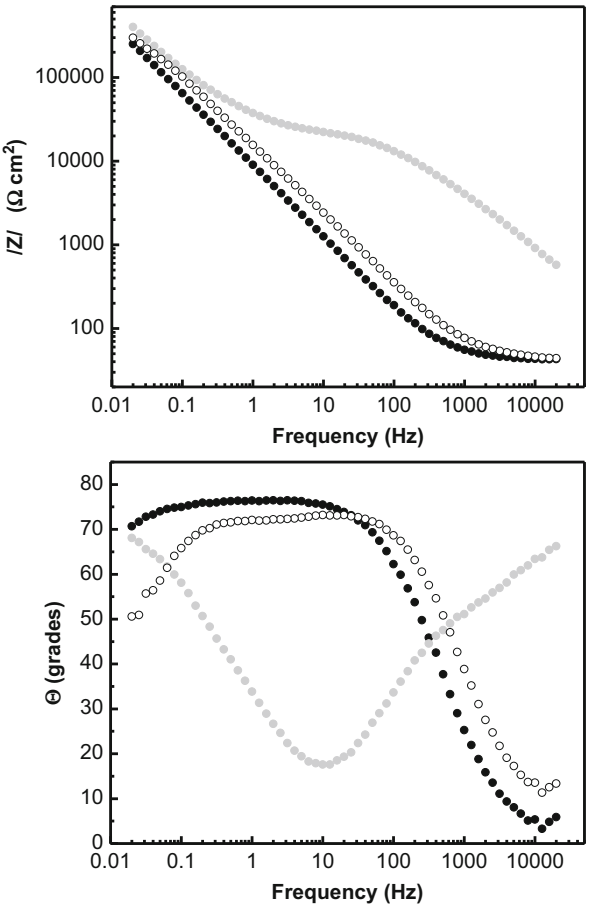

Fig. 12 Bode plots for **TEOS-MTES/TMH** after 1(◉) and 30 (o) days of immersion in SBF and their comparison with the bare stainless steel (●) (From López et al. (2008b))

beginning of immersion since its higher thickness that difficult the electrolyte reaching the substrate. However, this effect changes with immersion time.

Electrochemical impedance spectroscopy (EIS) is a nondestructive technique that can provide information about the on-going corrosion process. EIS studies the system response to the application of a periodic small amplitude ac signal. The measurements are carried out at different ac frequencies and that is why the name impedance spectroscopy was embraced. The system response permits to analyze information about the interface, its structure, and reactions taking place there (Lasia 1999). EIS assays show that the TEOS-MTES/TMH films provide a good protection to the bare substrate at the beginning of the immersion, but this film deteriorates after prolonged soaking probably due to the open structure provided by the TMH that favors the water uptake by the coating (Fig. 12). Although modeling of the data

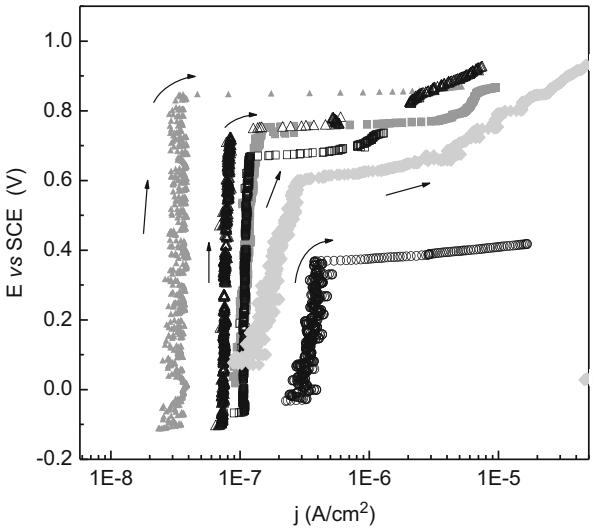

Fig. 13 Potentiodynamic curves for samples coated with TEOS-MTES with 10% of SiO_2 nanoparticles after 1 (Δ) and 30 (▲) days of immersion, samples coated with TEOS-MTES with 30% of SiO_2 nanoparticles after 1 (∇) and 30 (▼) days of immersion, and for the bare metal (•) after 30 days of immersion in simulated body fluid. The *arrows* indicate the direction of polarization

through the use of equivalent circuits permits connecting the impedance results with the physico-chemical parameters and it is a very powerful tool to analyze system behavior in time, this approach is not aroused in this chapter, but it can be found in the references cited herein.

As one of the main objectives to apply a coating onto the metallic substrate is to confer corrosion resistance, the barrier effect can be improved by adding silica nanoparticles to the sol as it was stated above. Figure 13 shows potentiodynamic anodic curves held for the coatings formulated using TEOS-MTES reinforced with SiO_2 nanoparticles either with 10% or 30% in weight in the first layer. Bare stainless steel and TEOS-MTES coating sample without SiO_2 particles with 30 days of immersion are included for the sake of comparison. It can be seen that there are not significant differences among the samples coated with TEOS-MTES reinforced with different amount of SiO_2 nanoparticles. The breakdown potential is between 0.7 and 0.9 V for both SiO_2-reinforced coatings at the two periods of time studied (1 and 30 days of immersion) and is higher than the values for the bare material and for the TEOS-MTES coating after 30 days of immersion. This fact could lead to a major corrosion resistance for this coatings comparing with the TEOS-MTES samples without nanoparticles or the bare metal. Current density remains almost invariant for all the studied systems, being around 1×10^{-7} A.cm^{-2}.

EIS assays show a slight deterioration of the coatings with time, showing a more corrosion resistance coating to the higher content of silica nanoparticles. The curves do not present big changes with increasing the immersion time in SBF, with an exception in the low frequencies zone where a raise in the phase angle with immersion time could be associated with a minor pores covering present in the coating (Fig. 14), proving the effectiveness of the barrier effect provided by this kind of reinforced coating.

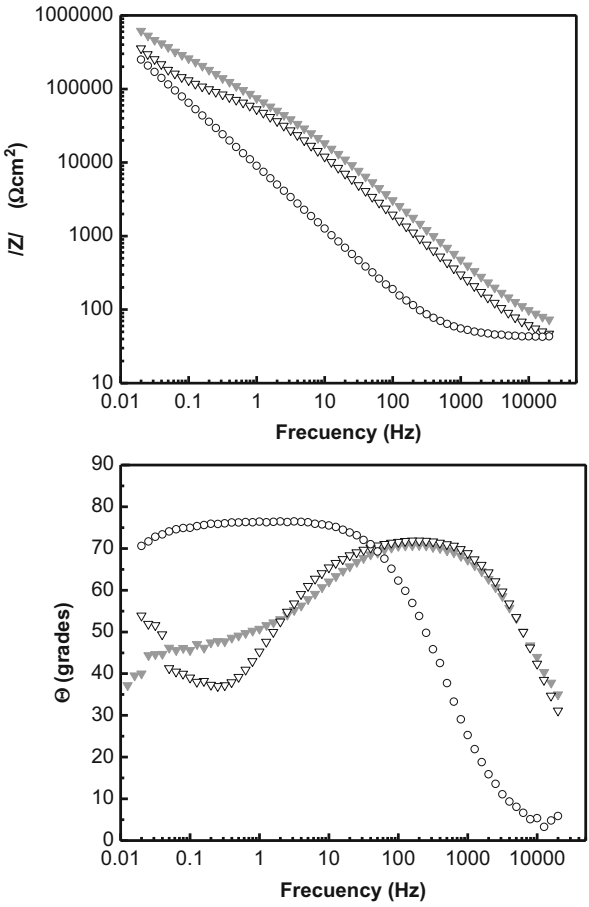

Fig. 14 Bode plots for TEOS-MTES-SiO_2 30% coatings on AISI 316L substrate after 1 (▼) and 30 (▽) days of immersion in SBF. Bare substrate was shown for comparison (○) after 30 days of immersion

Bioactivation of Stainless Steel Implants

Bioactive coatings are important for metallic implants such as hip prostheses and periodontal implants because some of the metals used as permanent implants (as stainless steel or CrCo alloys) are bioinert, which means they result encapsulated with fibrous tissue after implantation not creating a natural bonding to the living tissue (Hench and Wilson 1993). Bioactive coatings have the potential to improve the stability of implants by bonding them to the host bone where a hydroxyapatite (HA) layer forms as the result of the reaction of ceramic or glass bioactive particles (Jones 2013).

There are many strategies to bioactivate metallic surfaces. One strategy is the use of bioactive particles applied in the vehicle of a hybrid coating to be deposited onto the implant to use the excellent bioactivity of the bioactive particles as well as the advantageous mechanical properties of metals

(Cerruti et al. 2005; Galliano et al. 1998). Among the bioactive ceramics, Mg and Si-contained ceramics have attracted the attention as bone replacement materials (Ni et al. 2007). Si is an essential element in skeletal development and Mg is directly associated with mineralization of calcified tissues and with the mineral metabolism (Carlisle 1970; Matsko et al. 2011; Webster et al. 2004). Forsterite (Mg_2SiO_4) is a biocompatible material that presents bioactivity in vitro, better mechanical properties when compared to the hydroxyapatite, and can be applicable as a new biomaterial for hard tissue repairs. Kheirkhah et al. have proposed the use of forsterite coating by sol-gel method on AISI316L: the coating has an appropriate adhesion seems to be formed on the surface, whereas there is no evidence of presence in the gap between the forsterite coating and SS 316L substrate. Moreover, throughout the immersion test in simulated body fluid, coating delamination was not observed and the coating kept its integrity on the substrate until the end of the experiments. The forsterite coated samples not only exhibited a better corrosion resistance compared to the uncoated substrates but also shows the in vitro bioactivity (Kheirkhah et al. 2015).

Pourhashem and Afshar applied a double layer coating system containing a silica (SiO_2) intermediate layer and 45S5 bioglass (SiO_2–CaO–Na_2O–P_2O_5) top layer by sol-gel technique on AISI316L stainless steel substrates (Pourhashem and Afshar 2014). Several approaches have been used to evaluate the characteristics of the prepared coatings such as their phase structure, morphology, and corrosion resistance. After 7 days of exposure to SBF solution, the alkali and alkaline earth ions from the bioactive glass surface start to diffuse to the surrounding medium faster than ion precipitation on glass surface, leaving behind a corroded surface with increased surface area (Soundrapandian et al. 2011); thus, the corrosion rate increases in the first days of immersion. Further, leaching of ions leads to an exposition of Si–OH networked surface. This active surface stimulates the deposition of a thin film of hydroxyapatite on the bioactive glass surface which slowly reduces the exposed surface area. Thus, the pores and defects presented in the coatings could be blocked by corrosion products of the metal or by the degradation of the particles present in the coating. This blocking could cause a higher resistance to the diffusion of the electro-active species to reach the metallic substrate increasing the apparent resistance of the system with time and decreasing the rate of dissolution (Pourhashem and Afshar 2014).

Other compositions of bioglasses and microstructure of the final coatings can be obtained by the sol-gel method. Fathi and Doostmohammadi have prepared and characterized a bioactive glass nanopowder and developed a bioglass coating for improving biocompatibility of AISI316L stainless steel implants (Fathi and Doostmohammadi 2009). The composition of the bioactive glass belongs to the system CaO–SiO_2–P_2O_5 with 57.44% CaO, 35.42% SiO_2, and 7.15% P_2O_5 in molar percentages that was analyzed in first place by Galliano et al. (1998). The results showed that the size of bioactive glass powder was less than 100 nm. The formation of apatite layer confirmed the bioactivity of the bioglass nanopowder. The stainless steel AISI316L samples coated with bioactive glass showed higher Ebreak when compared with pristine samples. The authors concluded that AISI316L coated with

the bioactive glass as a human body implant can simultaneously offer an improvement in corrosion resistance together with biocompatibility and bone bonding.

Studies on biological behavior have demonstrated that zirconia (ZrO_2) and silica (SiO_2) create favorable response with good biocompatibility. Additionally, ZrO_2 exhibits high mechanical strength, high fracture toughness, and good corrosion resistance, making it a suitable protective material. Mieszek et al. studied the biocompatibility of zirconia-based coatings obtained by the sol-gel method. Two matrices, ZrO_2 and SiO_2/ZrO_2, were created and applied on AISI316L stainless steel by dip-coating technique. The results showed that the materials exerted different impact on mesenchymal stem cells (MSCs). The materials formulated with ZrO_2 layer were more biocompatible for adipose-derived MSCs, while SiO_2/ZrO_2 layer promoted proliferation of bone marrow derived MSCs. Moreover, hybrid coating exhibited greater osteoinductive properties than ZrO_2 coating, both on cultures with adipose-derived stromal (stem) cells and bone marrow stromal cells. The biological effects observed are a result not only from different chemical composition but also from the variation in wettability. The ZrO_2 coating resulted as a hydrophobic layer, while SiO_2/ZrO_2 exhibited hydrophilic properties. The results obtained suggest that behavior of MSCs in response to the biomaterial may vary depending on their origin (Mieszek et al. 2014).

Particles in Sol-Gel Coatings as Bone Promoting Agent

Protective and homogeneous coatings obtained by sol-gel can be functionalized to enhance induction and bone formation on the surface of stainless steel implants. As it was mentioned above, the development of hybrid organic–inorganic silica based coatings allow the incorporation of organic groups to the Si-O-Si structure, giving the film more plasticity and the capability to better adaptation to different roughness and substrates. Besides the addition of organic groups provide corrosion resistance and hydrophobicity to the layer (Amato 2001; Innocenzi et al. 1992). The bone induction functionality can be achieved by adding nano- or microparticles derived from bioactive glasses, glass ceramics, or ceramics. The incorporation of different particles with certain functionality have conducted systems with thicker coatings and bioactive response (Duran et al. 2004; Garcia et al. 2004).

The hybrid silica based coating with bioactive particles onto stainless steel implants has been studied by modifying the composition of the coating (de Damborenea et al. 1995; de Sanctis et al. 1990; Guglielmi and Zenezini 1990; Innocenzi et al. 1992; Pellegri et al. 1994) and the type or size of the particles contained in the coating (Ballarre et al. 2009c; de Sanctis et al. 1995; Gallardo et al. 2001; Galliano et al. 1998; García et al. 2003, 2006; Innocenzi et al. 1992; López et al. 2008b; Pellegri et al. 1994). Since the end of the 1990s, different particles were used in several silica based hybrid sols: from commercial hydroxyapatite, Hench bioactive glass® (Hench and Paschall 1973), glass-ceramics and apatite/wollastonite ceramics (Galliano et al. 1998; Garcia et al. 2004), wollastonite

(Ballarre et al. 2012) to 45S5 bioactive glass doped with cations like strontium (Omar et al. 2015). Strontium incorporation in ceramics and calcium phosphate cements for bone remodeling and repairing has been a topic of great interest in the last decade (Gorustovich et al. 2010; Kim et al. 2004; O'Donnell et al. 2010; Panzavolta et al. 2007). It has been demonstrated that calcium phosphate cements containing Sr are considered as osseous-progenitors since they promote the osteoblasts adhesion and proliferation, without showing decay in cellular adhesion, extracellular matrix formation, and in vitro mineralization (Gentleman et al. 2010). Also several studies showed that hydroxyapatite bone cements with Sr promote osteoblastic adhesion, in vitro mineralization, and also in vivo growth and osseointegration (Ni et al. 2006; Wong et al. 2004).

Coatings with Hydroxyapatite Particles

As one of the main mineral components of human bone is a modified form of hydroxyapatite this compound was one of the first to be considered as potentially bioactive. They could be commercially pure or synthesized via solid reaction, fusion, sol-gel, or precipitation route. Garcia et al. used this last kind of synthesis route for generating hydroxyapatite (HAp) particles. They were made from an aqueous solution of tetra hydrated calcium nitrate and ammonium phosphate, in concentrations 1 mol/L and 0.48 mol/L, respectively, in basic media (pH = 10), followed by a heat treatment of 1050 °C and milling (Garcia et al. 2004). About 10 wt% HAp particles were added to a TEOS-MTES sol (40:60 in mols) with a final concentration of SiO_2 of 200 g/L.

Garcia et al. (2004) obtained crack-free single and double coatings with homogeneous particle distributions and no observable defects (Fig. 15). The hydroxyapatite single coatings had a critical thickness around 2 μm and average particle size between 5 and 8 μm. Double layers were formed by an inner layer without HAp particles (1 μm thick) and the layer containing the HAp on the top of the first one. In vitro tests revealed that the coatings induced the formation of a semicrystalline hydroxyapatite (semi-HAp) rich layer onto the substrate surface as a result of the chemical reaction of the particles with the surrounding body fluid, considered as a preliminary signal of bioactivity after immersion in SBF (Kokubo et al. 1992). The coatings with HAp particles presented the first signal of in vitro HAp deposits after 72 h of immersion in simulated body fluid (Fig. 16). After 14 days of immersion in SBF, a minor area of the hydroxyapatite (HAp) containing coatings was covered by a semi-HAp film. It was found that comparing with other bioactive particles (glass ceramics and glass) the HAp presents lower reactivity.

The corrosion performance of single TEOS-MTES coating with HAp particles applied onto stainless steel substrates after 1 and 10 days of immersion in SBF can be seen in Fig. 17. The potentiodynamic curves and data corresponding to the HAp coatings at both immersion times show a decrease of the passivation current density (jpass), that is the current density to which the metal remains passive, and a shift to positive potentials of the breakdown potential (compared to the bare material). After

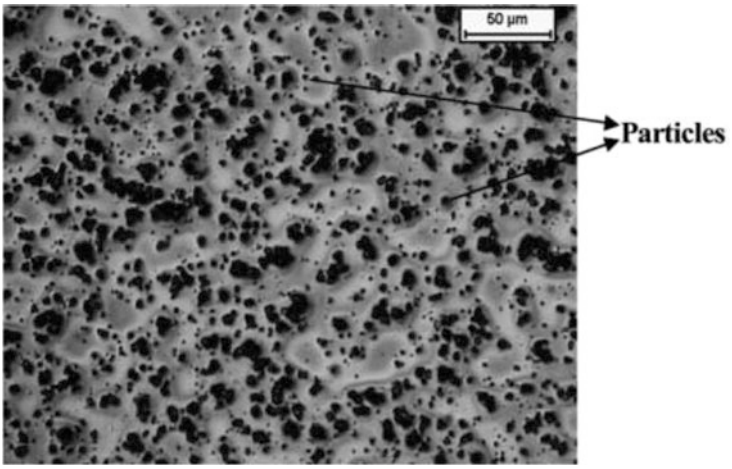

Fig. 15 Reflectance optical microscopy photographs of: hydroxyapatite containing coatings · 200 (From Garcia et al. (2004))

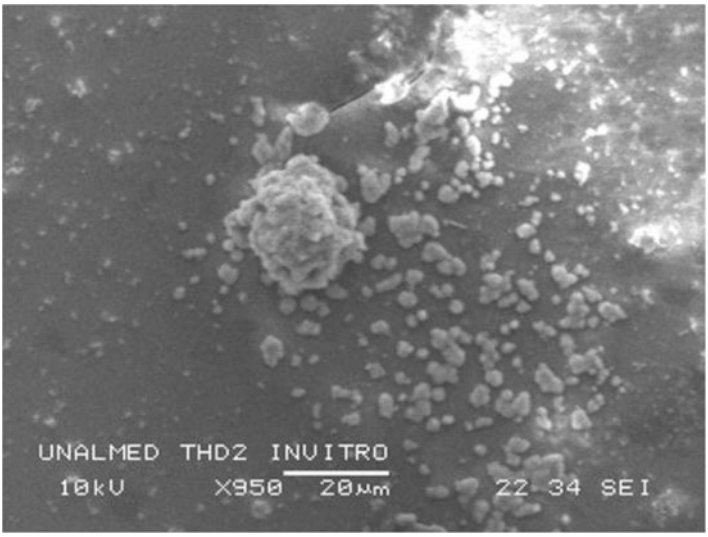

Fig. 16 SEM image of TEOS-MTES coating with hydroxyapatite particles after 72 h immersion in SBF, showing apatite deposits

10 days of immersion in SBF, the coating deteriorates and therefore the passive current intensities are bigger than in the initial time. This can also be observed in the EIS plots in the Bode form (Fig. 18) where after 10 days of immersion the total impedance decreases and there is drop in the phase angle at high frequencies (Garcia et al. 2004).

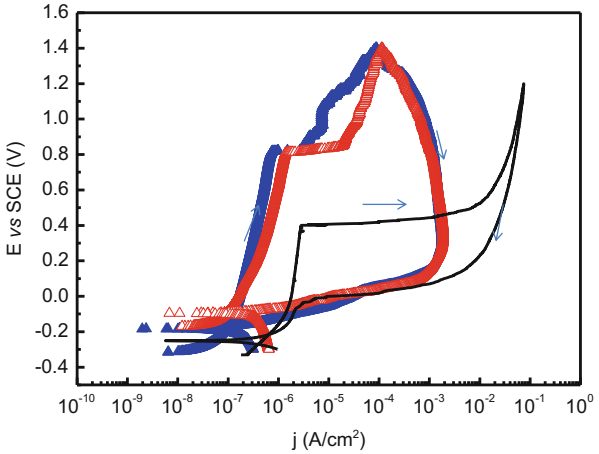

Fig. 17 Potentiodynamic curves of TEOS-MTES coating with hydroxyapatite particles on AISI316L substrate, after (▲) 1 day and (△) 10 days of immersion in simulated body fluid (*SBF*). The *solid line* corresponds to bare AISI316L substrate. The *arrows* indicate the direction of polarization

The silica based TEOS-MTES coatings containing hydroxyapatite particles applied onto stainless steel AISI 316L substrates were implanted for 90 days in Lewis rat femurs. The surrounding media did not present rejection signals, but no presence of new bone tissue was seen in the periphery of the implant (Garcia 2004). Bone resorption in vivo and poor stimulating effect on the growth of new bone tissues was also found by Buma et al., Collier et al., and Hardy et al. (Sun et al. 2001). Although the in vitro essays showed bioactivity of this type of coatings on stainless steel implants, the SBF soaking experiments do not certainly confirm the osseointegration in vivo of the system, as is deeply discussed by Bohner and Lemaitre (2009).

Coatings Containing Wollastonite Particles

Titanium implants coated with plasma sprayed wollastonite, $CaSiO_3$, (Liu and Ding 2002; Liu et al. 2001; Xue et al. 2005) or filled with wollastonite in powder form (Sahai and Anseau 2005) have been proven to have in vitro hydroxyapatite deposition ability, bone compatibility, osseoconductivity, and also bone inductivity in contact with bone marrow.

Ballarre et al. characterize a sol-gel TEOS-MTES coating with the addition of wollastonite particles as potentially bioactive particles on surgical grade AISI316L stainless steel in vitro in terms of bioactivity, corrosion response (Ballarre et al. 2012), and the in vivo osseointegration ability and the quality of the generated bone tissue around the implants (Ballarre et al. 2011). An apatite-like layer was formed on the surface of the TEOS-MTES-wollastonite coatings after immersion in

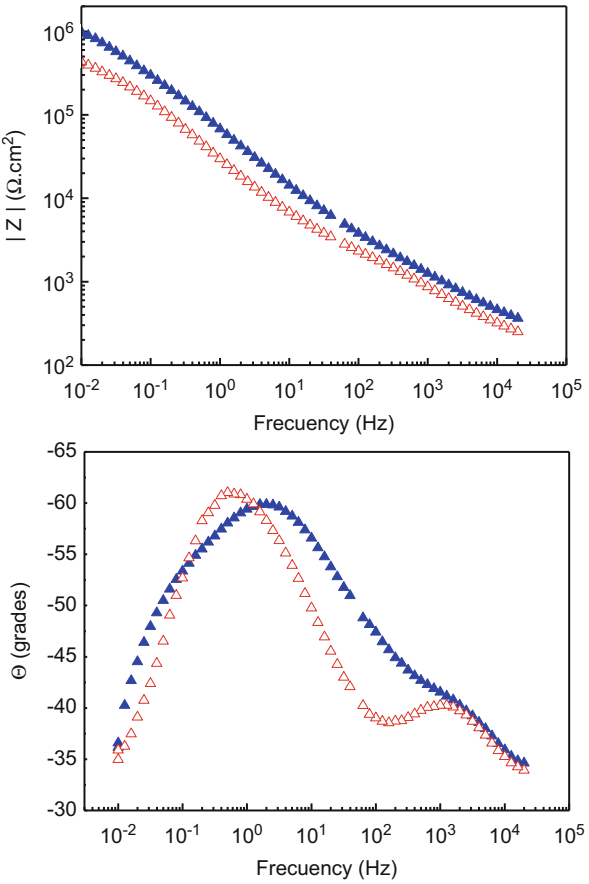

Fig. 18 Bode representation curves of TEOS-MTES coating with hydroxyapatite particles on AISI316L substrate, after (▲) 1 day and (△) 10 days of immersion in simulated body fluid (*SBF*)

SBF. Dissolution of the wollastonite particles provides Ca and P enrichment of the deposited phase, hence enhancing solidification (Hastings 1980; Zhang et al. 2003). After 5 days of immersion, the deposition starts with cracking and dissolution around the wollastonite particles within the TEOS-MTES coating (Fig. 19). This is due to the reaction between the calcium and the hydrated silica ions that provides favorable sites for apatite nucleation and an increase in the ion activity product of the apatite in the surrounding body fluid (Garcia et al. 2004; Hench and Wilson 1993; Kokubo et al. 1992). After 33 days of immersion, the deposited phase presented a homogeneous island-shaped appearance (Fig. 19a).

The corrosion behavior of the coated materials was studied in comparison to the bare material by potentiodynamic assays and electrochemical impedance

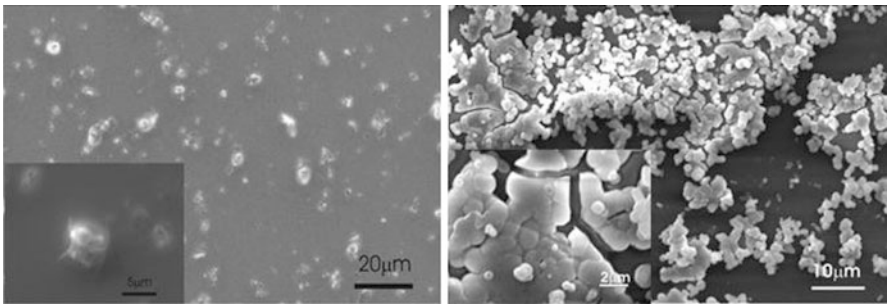

Fig. 19 (**a**) Morphologic aspect of the double layer coating with 10% of dispersed particles of wollastonite after 5 days of immersion in SBF. (**b**) SEM image of the precipitate formed on the double layer coating with 10% of dispersed particles of wollastonite after 33 days of immersion in SBF (From Ballarre et al. (2012))

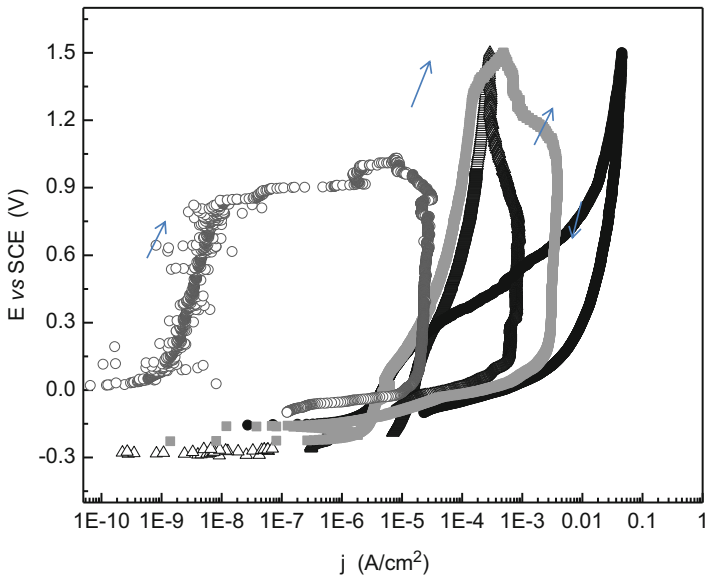

Fig. 20 Potentiodynamic polarization curve for the TEOS-MTES coating with wollastonite particles after 1, 7, and 40 days of immersion in SBF. • stainless steel, ○1 day, Δ 7 days, ■ 40 days. The *arrows* indicate the direction of polarization (From Ballarre et al. (2012))

spectroscopy. Figure 20 shows the potentiodynamic polarization curve for the TEOS-MTES coating with wollastonite particles after 1, 7, and 40 days of immersion in SBF and its comparison with the bare material. After 1 day of immersion, the coated material presented a low current density showing a blocking and protective behavior of the TEOS-MTES coating with wollastonite particles. After 7 and

40 days of immersion, the measured current density does not show noticeable differences when comparing the coated with the bare material. However, an enhancement in the breakdown potential is observed for the coated samples, not showing localized corrosion in the range of potentials under study.

Figure 21 shows the EIS plots in Bode representation of the samples coated with TEOS-MTES containing wollastonite particles and a comparison with the bare

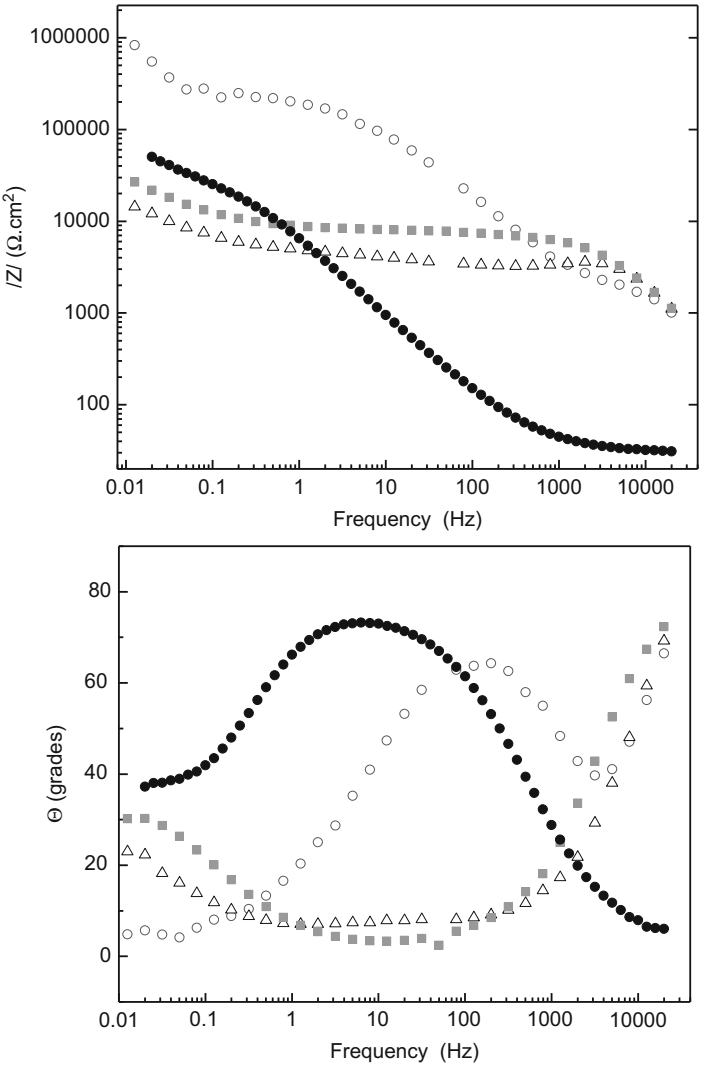

Fig. 21 Bode graphs representation for the SS316L substrate, TEOS-MTES coated materials with wollastonite particles after 1, 7, and 40 days of immersion in SBF. • stainless steel, ○ 1 day, Δ 7 days, ■ 40 days (From Ballarre et al. (2012))

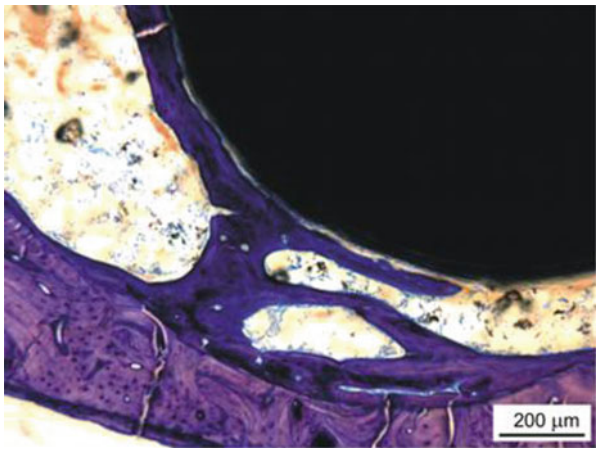

Fig. 22 Optical microscopic images of Giemsa stained histology sections showing the coated implant and the newly formed bone for 10× after 60 days of implantation in rat femur (From Ballarre et al. (2012))

stainless steel. After 1 day of immersion, the coated material presents a highly capacitive behavior showing high total resistance impedance that could be related with the coating integrity. With the increase in the immersion time (7 days), the coatings present a notorious general deterioration due to the breaking and dissolution of the particles in the coating. After 40 days of immersion in SBF, the system showed a similar behavior than after 7 days due to continuous cracking of the coating and the porous Ca/P compounds deposition on the created defects (Keding et al. 2002). When comparing coated with uncoated samples, the barrier effect provided by the sol-gel coating showed to improve the resistance to localized corrosion although the current density after prolonged immersion remains constant.

In vivo studies (Fig. 22) reveal the newly formed bridge-like bone tissue that can be seen between the implant and the existing cortical bone endostium; this is known as the remodeling zone between the implant and the old cortex bone. Newly grown bone tissue can be identified around the implant growing perpendicular to the longer axis of the implant and perpendicular to the existing cortical bone in contact with the bone marrow.

Coatings Containing 45S5 Bioglass (BG) Particles and 45S5 Partially Substituted with Strontium (Sr)

Bioceramics and specially bioactive glasses are produced in a variety of forms and phases and have different functions, where the most common is as material for filling defects (Hench and Wilson 1993). Glasses from the system SiO_2–P_2O_5–Na_2O–CaO have been studied since L. Hench presented the bioactivity that they show in 1973 (Hench and Ethridge 1982; Hench and Paschall 1973). The so-called Bioglass® (45S5) bioactive glass is a melt-derived glass composed of 45% SiO_2, 24.5% Na_2O, 24.5% CaO, and 4% P_2O_5 (weight percentages) and is used clinically as bone-regenerative material in dental and orthopedic applications.

Thanks to its positive effects on bone biology, the incorporation of strontium (Sr) in ceramic and calcium phosphate cements has been a topic of great interest in the last decade (Fujikura et al. 2012; Gorustovich et al. 2010; Kim et al. 2004; Panzavolta et al. 2007). Strontium-containing agents have been shown to inhibit bone resorption by osteoclasts and promoting osteoblast replication and bone formation (Marie 2005). It has been demonstrated that calcium phosphate ceramics containing Sr can be considered as bone-precursors since they promote adhesion and osteoblasts proliferation, showing no deterioration and slow degradation with time caused by cell adhesion, extracellular matrix formation, and mineralization in vitro (Gentleman et al. 2010). Several studies showed that hydroxyapatite bone cements containing Sr promote osteoblast adhesion and mineralization in vitro (Strobel et al. 2013) as well as growth and bone integration in vivo (Li et al. 2010; Newman et al. 2014; Ni et al. 2006; Wong et al. 2004). Because of similarities in their charge and ionic radius, strontium can potentially be substituted for calcium in BG, creating a material that may combine the bone bonding and osteoblast stimulating properties of BG with the bone anabolic and anticatabolic properties of strontium ranelate and may act as an effective material for bone regeneration applications.

Omar et al. studied the incorporation of Sr to a classic 45S5 BG and obtained a "BGSr" (that means bioglass with 2% in mol of the Ca substituted by Sr). The particles obtained in the same way of the BG were incorporated into a TEOS-MTES with SiO_2 nanoparticles (TMS) sol-gel coating and applied onto AISI316L (Omar et al. 2015). Raman spectra were measured before and after the exposition of the samples to the simulated body fluid for 30 days (Fig. 3a) to detect the formation of HAp. As it was expected, no presence of apatite-related compound were found for the samples before immersion, and the presence the bands related to the BG particles were not found, meaning that the particles remained below the coating. After 30 days of immersion, new bands appeared that were associated to carbonated HAp (Fig. 23) (Carden and Morris 2000).

Figure 24 shows the potenciodynamic assays for the coated samples. They presented current density three decades lower than the bare steel after 1 h of immersion with no signals of breakdown potential in the range of potentials. After 30 days of immersion, current densities of all the coated systems remained 2 orders of magnitude lower than the stainless steel, indicating that – even though there is a slight deterioration of the coatings due to particle release and dissolution – the coatings still remain protective when compared with the bare stainless steel. Electrochemical impedance spectroscopy (EIS) tests in the same experimental conditions than the previous ones are shown in Fig. 25. All the coated systems presented in the early stages of immersion show a total impedance modulus between 4 and 5 orders of magnitude higher compared with the bare metal. The phase angle θ vs. frequency Bode plot of the samples after 1 h of immersion shows a very plane curve with a decreasing tendency without reaching the zero value at low frequencies for the TMS, TMS-BG, and TMS-BGSr coatings. This could be related with a film with high

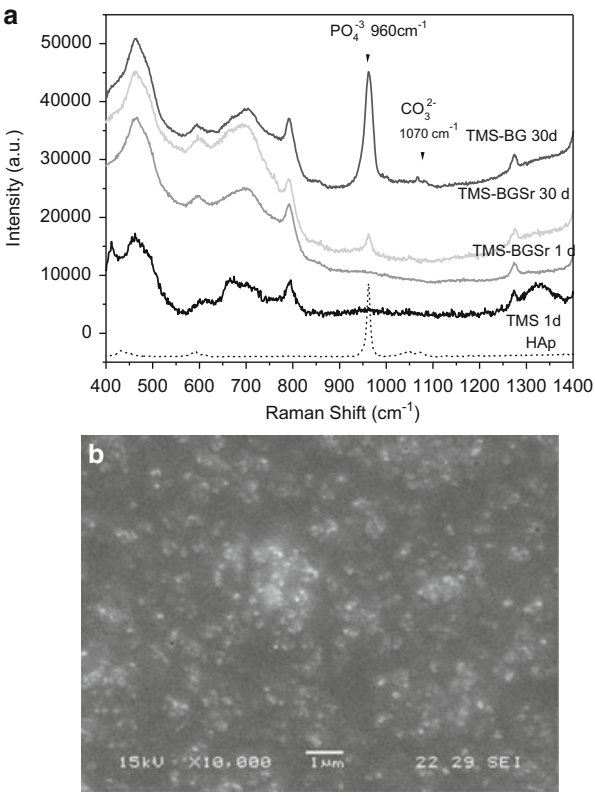

Fig. 23 (**a**) Raman spectra of the analyzed coatings (TMS, T-BG, and T-BGSr) with and without immersion in SBF. The hydroxyapatite spectrum (*HA*) is shown as a reference; (**b**) SEM image of the T-BG surface after 30 days immersion in simulated body fluid (From Omar et al. (2015))

integrity, with a capacitive behavior at high frequencies. After 30 days of immersion two time constants can be observed for the coated systems. A deterioration of all coatings can be noticed since the systems lose their capacitive behavior with a shift of the high frequency time constant. It is noticeable that coated substrates containing BGSr particles show more signs of deterioration than the ones with BG particles. This can be as result of Ca ion substitution by Sr ions in the glass network introducing tensions since Sr ions are slightly bigger than the Ca ones. As a result, this distortion could increase the rate of dissolution of the BGSr particles compared to the BG ones (O'Donnell et al. 2008; O'Donnell and Hill 2010) introducing more defects to the coating during dissolution.

Figures 26a, c and 24b, d show environmental scanning electron microscope (ESEM) images of femurs of Wistar rats after having AISI316L stainless steel implants coated with TMS with BG and BGSr for 4 weeks. It can be observed newly grown bone tissue around the implants growing in contact with the bone marrow with a growing direction perpendicular to the longer axis of the nail-like implant. Both coatings (TMS-BG and TMS-BGSr) presented good osseointegration

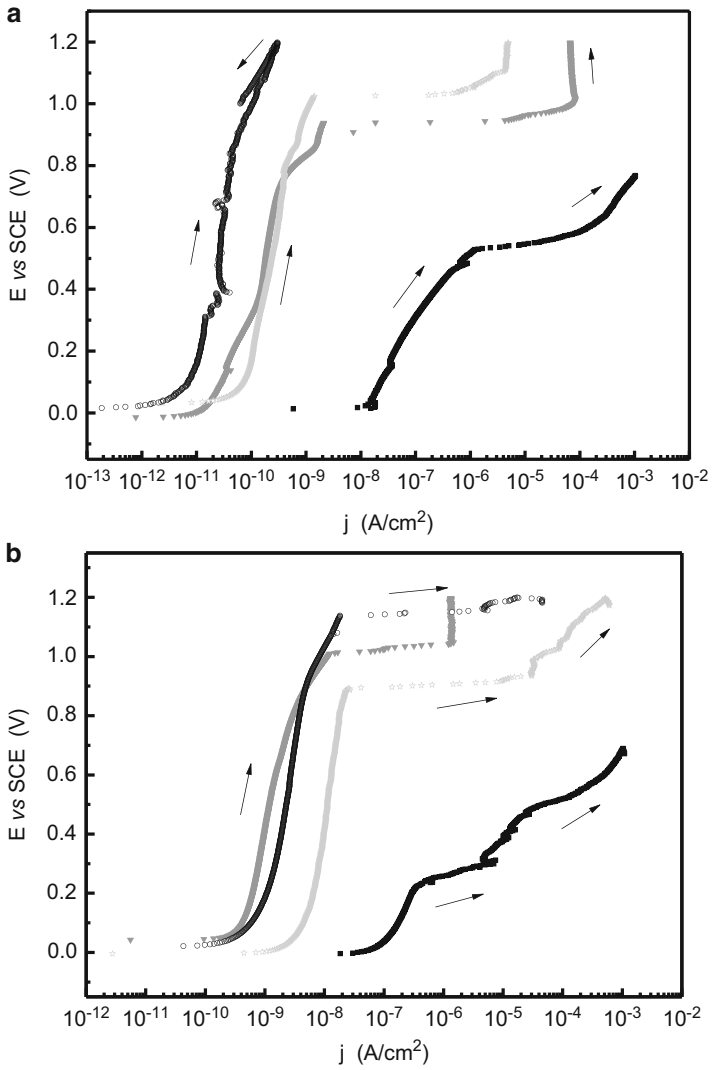

Fig. 24 Potentiodynamic polarization curves for all conditions of study (**SS** ■, **TMS** ○, **TMS-BG** ▼, and **TMS-BGSr** ⋆ coatings) (**a**) after 1 h of immersion and (**b**) after 30 days in SBF at 37 °C. The *arrows* indicate the direction of polarization (From Omar et al. (2015))

and bone regeneration behavior around the coated materials in a rat model. At early stage of bone regeneration, the thickness of the bone tissue formed around TMS-BGSr implants is slightly bigger but not statistically different. By micro Raman spectroscopy and data analysis (Ballarre et al. 2013; Bi et al. 2011;

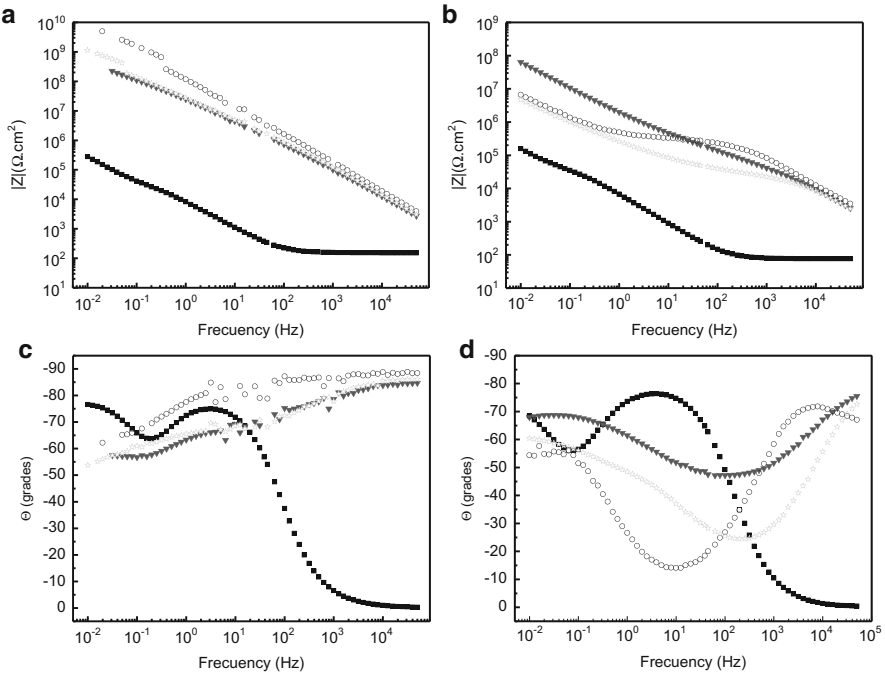

Fig. 25 Electrochemical impedance spectroscopy Bode representation plots for all studied conditions: **SS** ■ bare metal, **TMS** ○ coating, **TMS-BG** ▼ coating, and **TMS-BGSr** ⋆ coating after 1 h of immersion (**a** and **c**) and after 30 days in SBF at 37 °C (**b** and **d**) (From Omar et al. (2015))

Gamsjaeger et al. 2010; Kazanci et al. 2006), the content of phosphate in the matrix can be calculated to settle the relationship between organic matrix and mineral content as beta carbonate substitution in order to see the tissue maturity. The coatings containing Sr presents better mineralized characteristics as a mature and stable tissue.

Coatings Containing Glass-Ceramic (GC) Particles

Other type of bioactive particles that can be added to silica based sol-gel coatings on stainless steel implants for enhancing osseointegration are partially crystallized glasses, so-called glass-ceramic particles. Garcia et al. and Ballarre et al. have used glass-ceramic particles made from a precursor glass of the system SiO_2–P_2O_5–CaO (CaO of 47.29%, SiO_2 35.69% and P_2O_5 17.01% in weight in the final glass) (Ballarre et al. 2008b; Garcia et al. 2004, 2006). Two particle size distributions were used: (a) “small particles” (s.p.) for particles with diameter less

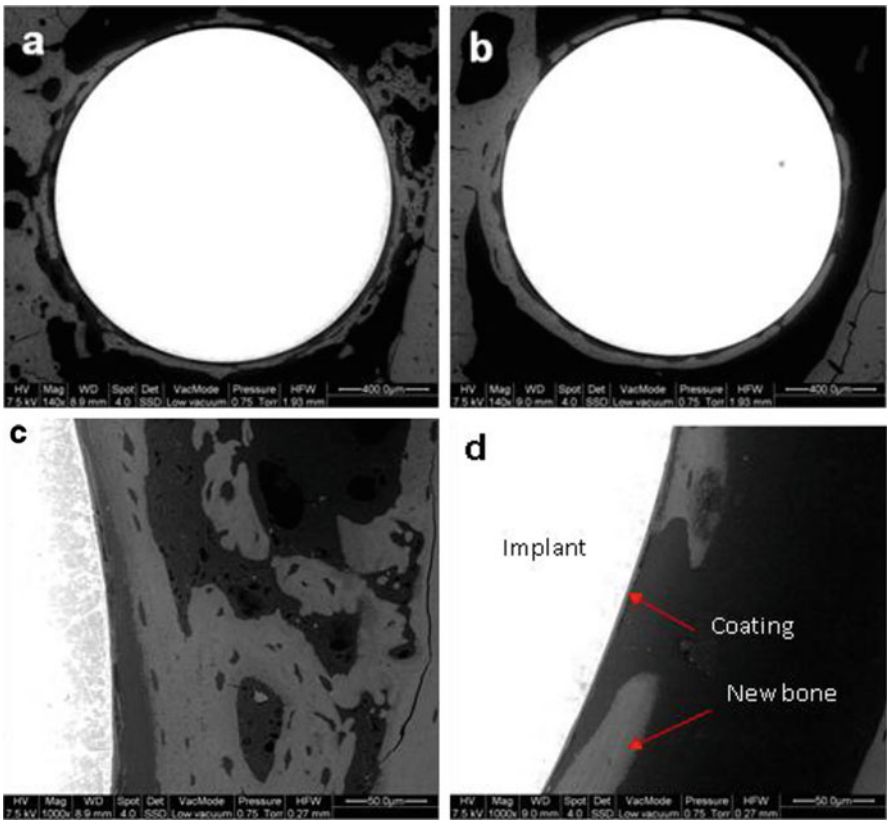

Fig. 26 Back scattering ESEM of (**a**, **c**) T-BG and (**b**, **d**) T-BGSr coated samples 4 weeks after implantation in rat femur. A detail of the different parts of the system implant/coating/bone was shown with *arrows* in (**d**) (From Omar et al. (2015))

than 20 μm and (b) "big particles" (b.p.) for particles with diameter bigger than 20 μm but smaller than 45 μm. The particle suspensions were prepared by the addition of 10% in weight of particles with respect to the solution (García et al. 2005).

Coatings were obtained by the dip-coating technique at room temperature and withdrawn at 25 cm/min. Two different types of coatings were used in this work: (1) TMH/TMH: this consist in two layers of TMH followed by a third layer of TMH containing a suspension of 10% weigh in volume of bioactive particles (some samples with small particles and some with big ones); (2) TEOS-MTES/TMH: this consist in a single layer of TEOS-MTES treated at 450 °C during 30 min, and then a second layer deposited on top of if consisting in two layers of TMH hybrid, followed by a third layer of TMH containing a suspension of 10% weigh in volume

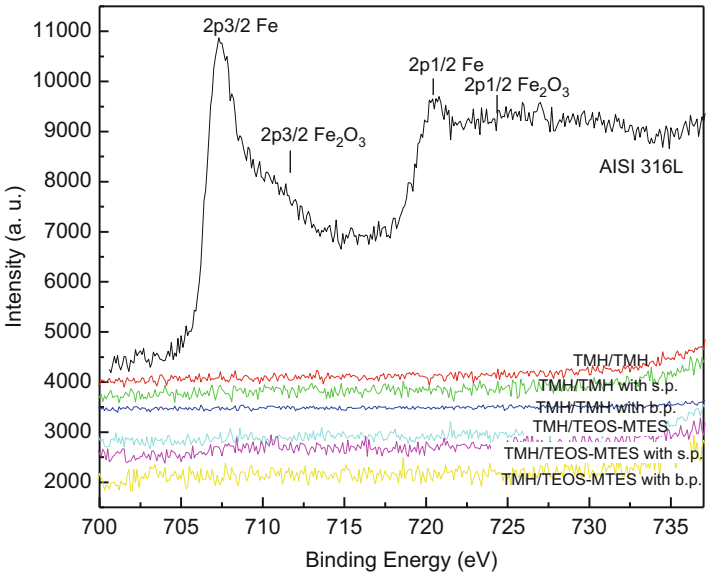

Fig. 27 X-ray photoelectron spectroscopy (*XPS*) high resolution scans for Fe 2p of the TEOS-MTES, TEOS-MTES/TMH, and TMH coatings on AISI316L stainless steel (From Ballarre et al. (2007b))

of bioactive particles (either small or big particles). All coatings were heat treated at 150 °C for 60 min in air atmosphere.

In vitro integrity, corrosion resistance, and bioactivity were analyzed after immersion in SBF at 37 °C for 30 days. Figure 27 presents the high resolution XPS scans for Fe 2p region after 30 min sputtering with Ar^+ ions. The TEOS-MTES/TMH and TMH/TMH samples immersed for 30 days in SBF did not present Fe ions neither on the coatings without particles or on the samples with the two sizes of particles for both coating system. The same kind of results were found in the Ni 2p and Cr 2p regions after 30 min of sputtering (not shown). Only the samples without any coating (base stainless steel) presented the characteristic peaks of Cr, Fe, and Ni. These results show that the metallic ions of the substrate did not migrate across the coating after 30 days of immersion in SBF. It could also be assumed that the film is not degraded enough as to detect the presence of the metallic substrate.

Figure 28 SEM micrographs of the surface films with TEOS-MTES/TMH coating with small particles after 24 h and 30 days of immersion in SBF are shown as an example. It can be observed the deposition of a higher proportion of HAp deposition than the samples with big particles (Ballarre et al. 2007b). The same kind of results is observed for TMH/TMH coatings (not shown). The analysis of these results by the watershed transformed essays show a HAp density of 53.9%

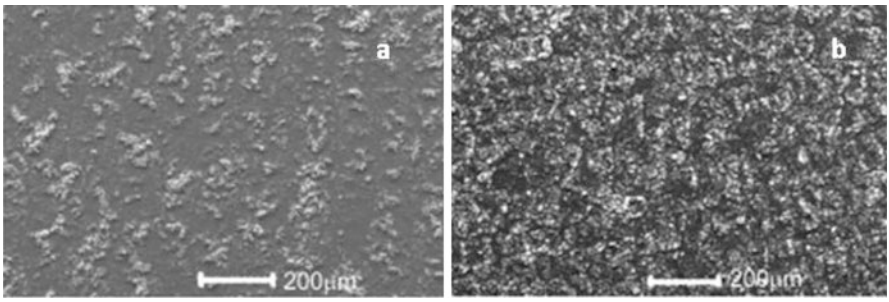

Fig. 28 Surface morphology of TEOS-MTES/TMH coating on stainless steel 316L with small particles, after (**a**) 24 h and (**b**) 30 days of immersion (From Ballarre et al. (2007b))

and 57.5% for the samples with TMH/TMH and TEOS-MTES/TMH coatings with small particles, and a particle density of 39.5% and 32.7% for the same coated samples with big particles.

Nevertheless, in vitro tests revealed that all the coating containing particles induced the formation of HAp as a result of the chemical reaction of the particles with the simulated body fluid. As the coatings containing small particles present a higher reactive area, it is not surprising that they are able to induce a higher proportion of HAp deposition on the surface, than the big ones. This fact may lead to the assumption that smaller particles could be considered to have a better bioactive response than bigger particles. However, it is important to consider another aspect related to these coatings that is the protective function. It has been already studied (Garcia et al. 2004, 2006) that the particle reaction to form HAp breaks the coating that contains the particles inducing cracks in the surrounding of the particle. This fact could lead to localized corrosion of the substrate if the flaws reach the substrate.

It is also important to note that the first layer of TEOS-MTES or TMH applied to the AISI316L substrates does not affect the bioactive response of the samples. The effect of the protective barrier provided by the first layer coating should enhance the corrosion resistance of the substrate when compared with the single layer.

Potentiodynamic curves of the TMH samples either with small or big particles have a similar behavior after 30 days of immersion in SBF. Current density around corrosion potential and breakdown potential for the coated samples are almost the same of the naked material, showing no improvement in the coating protective behavior. Only a slight decrease in the current density of the TMH with big particles coated sample after 30 days of immersion is observed. The dual TEOS-MTES/TMH coating containing small particles shows similar current density than the bare alloy although the breakdown potential shifts anodic for the coated material. The system TEOS-MTES/TMH coating containing big particles shows decay in current density after 30 days of immersion. The dual coatings with TEOS-MTES and TMH present

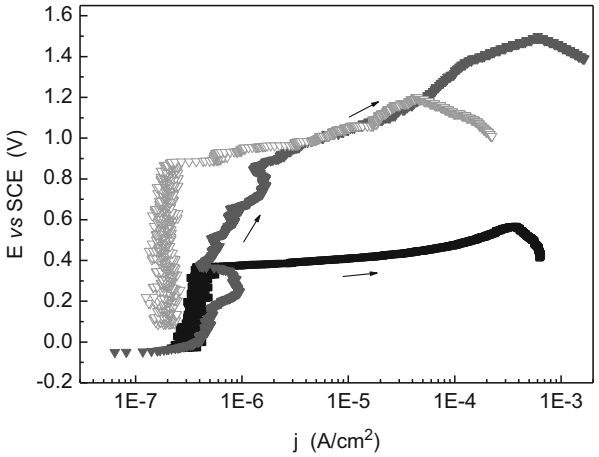

Fig. 29 Potentiodynamic polarization curve of the TEOS-MTES/TMH coating containing big particles after 1 (▼) and 30 (∇) days of immersion in SBF, and their comparison with the bare alloy (■). The *arrows* indicate the direction of polarization (From Ballarre et al. (2008b))

larger breakdown potential than the TMH ones because of the presence of an inner more inorganic protective film (TEOS-MTES), but the current density remains comparable to the bare material around the corrosion potential (Amato et al. 2005; Gallardo et al. 2001; Garcia et al. 2004; Fig. 29). Those results show that although there is slight improvement in the corrosion resistance with the double coating array, this improvement is not enough since the current densities in the surrounding of the corrosion potential are comparable to the bare material. The electrolyte reaches the substrate probably through defects created with the incorporation of the bioactive particles.

As it was previously pointed out, it is of major importance to increase the barrier effect of the coating to enhance the corrosion resistance of the substrate. Nanoparticles of SiO_2 added to the sol reinforce the films filling the defects and holes present in the silica network, thereby decreasing the porosity and the conductivity of the surface. Double layers of TEOS-MTES with silica nanoparticles as inner layer and the adding of bioactive glass-ceramic particles in the top layer were studied by Ballarre et al., applied onto AISI316L. The authors studied the in vitro bioactivity of coated samples by analyzing the formation of bone like apatite on the surface after immersion in SBF (Kokubo et al. 1992) by XPS. High resolution spectra of the distinctive elements of apatite: Ca, P, and O were measured and quantified by comparing the proportion of the peaks area (Fig. 30). The calculated value of Ca/P ratio for the GC particles was 3.86, whereas for coating containing GC after immersion in SBF it was 1.43. The standard stoichiometric hydroxyapatite (HA) has a Ca/P ratio of 1.67 (Ballarre et al. 2009c). In addition, O/P and O/Ca

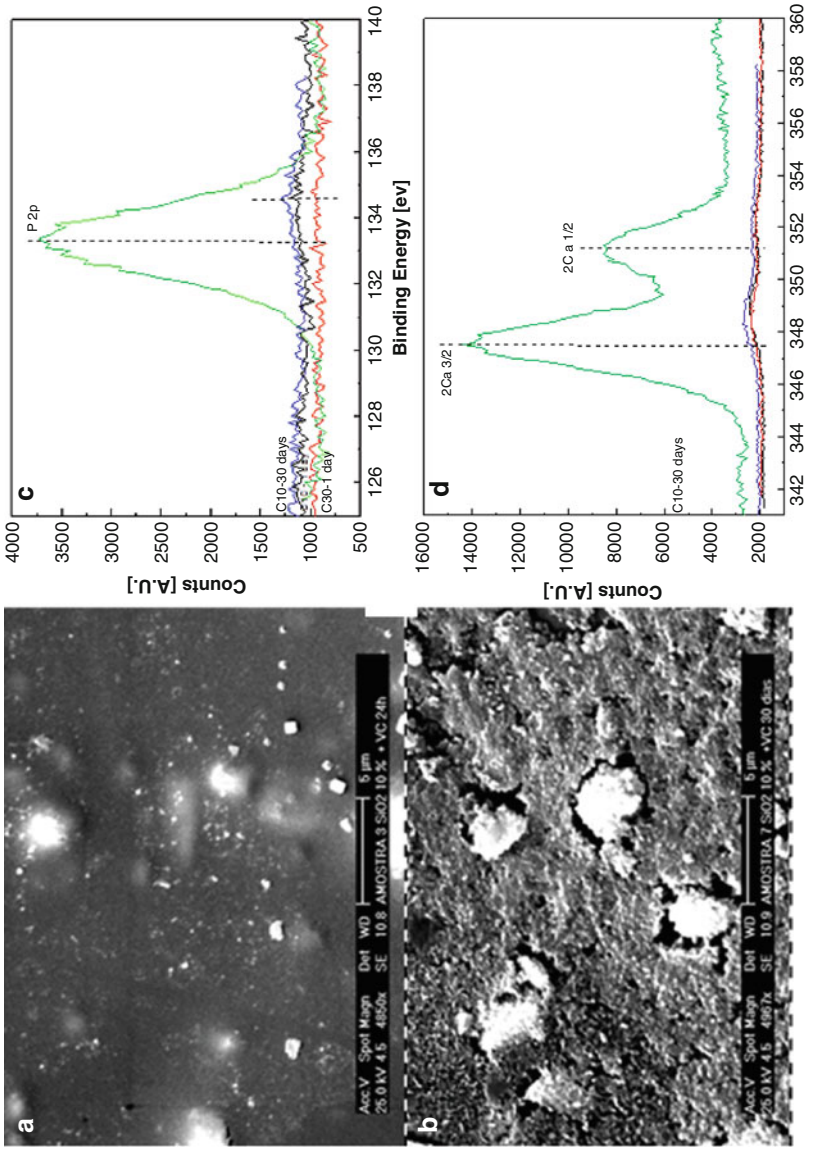

Fig. 30 Scanning electron microscopy (*SEM*) for TEOS-MTES-SiO_2 coatings with 10% of SiO_2 on AISI316L substrate with: (**a**) 1 day and (**b**) 30 days of immersion in SBF. (**c**) X-ray photoelectron Spectroscopy (*XPS*) high resolution scans for Ca1s and (**d**) P2p elements

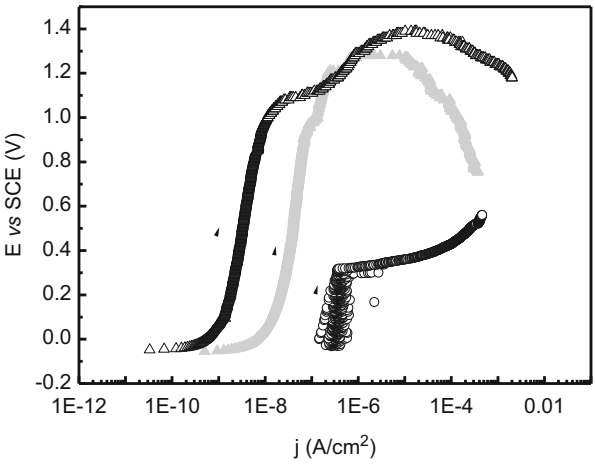

Fig. 31 Potentiodynamic polarization curves for the TEOS-MTES-SiO_2 10% coating on AISI316L after 1 day (▲) and 30 days (Δ) of immersion in SBF at 37 °C

ratio values for the samples immersed in SBF were 4.13 and 2.88, slightly different from the stoichiometric HA that has values of 4.33 and 2.6, respectively. The values obtained for the samples support the HAp dissolution/redeposition theory conducted by Kokubo et al. (2003), Peitl et al. (2001), and Li et al. (1996) which state the beginning of dissolution of glass-ceramic materials forming partially crystallized apatite and wollastonite phases, obtaining apatite-like deposits after immersion in SBF for a period of time. The deposition and formation mechanism of apatite like layer and its composition depends largely on the substrate and the media content. The substrates in which the apatite layer is deposited can also be activated by adding functional groups that help in apatite nucleation. Therefore, the use of a silica based coating supporting the GC particles is a way to improve the coating and increase the bioactivity of the stainless steel surfaces in vitro (Ballarre et al. 2010).

Potentiodynamic tests after 24 h and 30 days of immersion in SBF at 37 °C were conducted in order to evaluate corrosion resistance of the coatings after immersion (Fig. 31). It is important to note that current density remains lower than for the bare material and after 30 days of immersion in SBF the current density is even reduced, probably due to a decrease in the expose area due to the presence of deposits onto the surface. The same tendency is observed in EIS assays shown in Fig. 32 where it can be noted that the dual coatings present a high total resistance. The system containing 10% of silica nanoparticles in the TMS layer shows no degradation with time, showing an improvement in its protective performance. This could be due to the deposition of HAp onto the surface, covering flaws and pores created by GC dissolution with immersion time. This is in good agreement with the previously shown potentiodynamic experiments, where a reduction of current density was observed. When higher concentration of nanoparticles is used in the inner layer (30%SiO_2) this effect is not perceived and slight grade of deterioration is observed after prolonged immersion (Ballarre et al. 2009c).

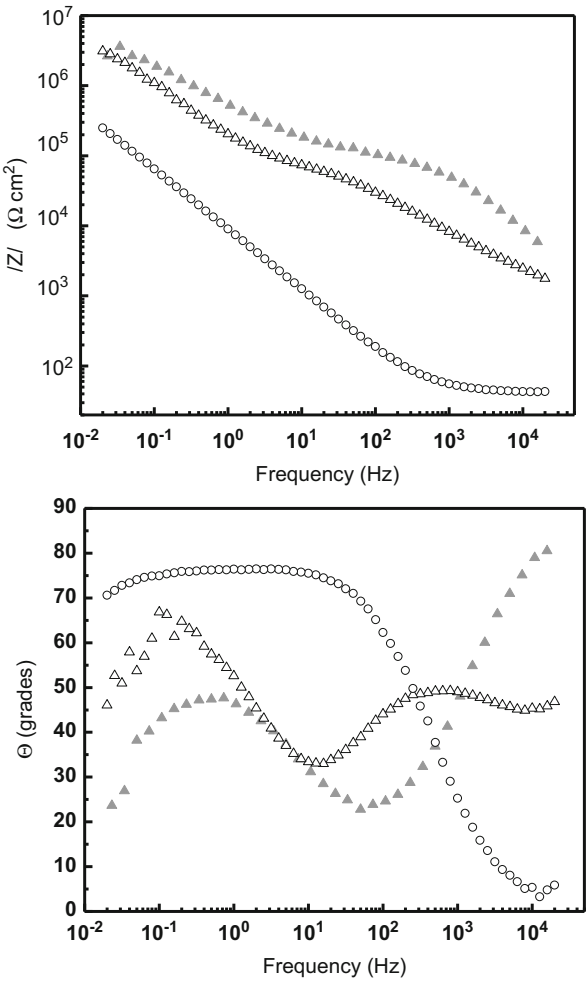

Fig. 32 Bode representation plots for the TEOS-MTES-SiO_2 10% coating on AISI316L substrate after 1 (▲) and 30 (Δ) days of immersion in SBF. Bare AISI 316L is shown for comparison (○)

The implantation of these materials in Wistar rats for 60 days shows bioactive response in vivo, where the formation of new bone can be observed in the surrounding of the implant (Fig. 33).

The protection and functionalization of AISI 316L stainless steel with hybrid silica based coating of TEOS-MTES with SiO_2 nanoparticles and loaded with bioactive glass ceramic particles can be achieved. The improvement of the implant material as bioactive materials has been proved in vitro and also in vivo, with the decrease in corrosion processes and bone formation.

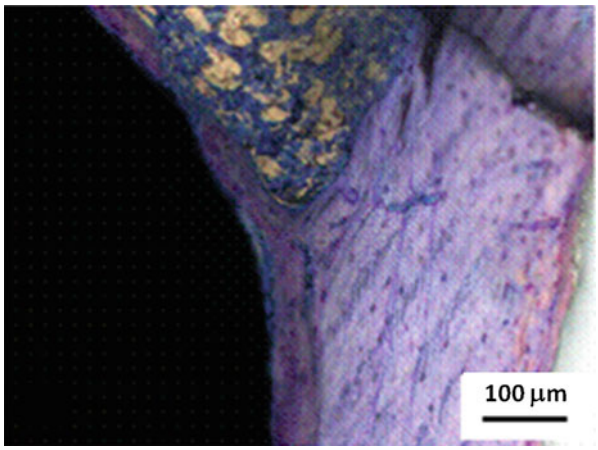

Fig. 33 Optical microscopic image of a Giemsa stained histology section showing the implant and the newly formed bone around coated stainless steel with TEOS-MTES-SiO2 10% sample after 60 days of implantation in rat tibia

Conclusion

The AISI 316L stainless steel is often used as permanent implant in orthopedic surgery although it is susceptible to localized corrosion in body fluids. As in situ degradation of permanent implants is an undesirable phenomenon, all efforts tending to minimize the detrimental effect of the host on the metallic substrate are of great value. When cementless prosthesis is used, osseointegration is a requirement to be achieved. Sol-gel coatings applied onto AISI 316L stainless steel have been successfully proved to prevent corrosion of the metal, and furthermore, it can be functionalized with different classes of bioactive particles in order to promote bone regeneration. The improvements have been demonstrated in vitro and in vivo, being a promising system to go a step forward in the clinical assays as a functionalized material for orthopedic implants.

Acknowledgments The authors would like to thank very specially Prof. Alicia Duran and Dr Claudia Garcia for the cooperation activities. Also to the National University of Mar del Plata (UNMdP) and the National Research Council (CONICET) for the support, and all the students, technicians, researchers and fellows involved in the experimental development of this project.

References

Amato L. Preparación y evaluación electroquímica de recubrimientos híbridos por sol–gel sobre aleación de Co-Cr-Mo de uso clínico. Proyecto final, Facultad de Ingeniería, UNMdP, Mar del Plata; 2001.

Amato LE, López DA, Galliano PG, Ceré SM. Electrochemical characterization of sol–gel hybrid coatings in cobalt-based alloys for orthopaedic implants. Mater Lett. 2005;59(16):2026–31.

Atanacio AJ, Latella BA, Barbé CJ, Swain MV. Mechanical properties and adhesion characteristics of hybrid sol–gel thin films. Surf Coat Technol. 2005;192(2–3):354–64.

Balamurugan A, Sockalingum G, Michel J, Fauré J, Banchet V, Wortham L, Bouthors S, Laurent-Maquin D, Balossier G. Synthesis and characterisation of sol gel derived bioactive glass for biomedical applications. Mater Lett. 2006;60(29–30):3752–7.

Balamurugan A, Balossier G, Kannan S, Michel J, Faure J, Rajeswari S. Electrochemical and structural characterisation of zirconia reinforced hydroxyapatite bioceramic sol–gel coatings on surgical grade 316L SS for biomedical applications. Ceram Int. 2007;33(4):605–14.

Ballarre J, Orellano JC, Bordenave C, Galliano P, Ceré S. In vivo and in vitro evaluation of vitreous coatings on cobalt based alloys for prothetics devices. J Non Cryst Solids. 2002;304(5):278–85.

Ballarre J, López DA, Cavalieri AL. Nano-indentation of hybrid silica coatings on surgical grade stainless steel. Thin Solid Films. 2007a. https://doi.org/10.1016/j.tsf.2007.07.186.

Ballarre J, López DA, Schreiner WH, Durán A, Ceré SM. Protective hybrid sol–gel coatings containing bioactive particles on surgical grade stainless steel: surface characterization. Appl Surf Sci. 2007b;253(17):7260–4.

Ballarre J, López DA, Cavalieri AL. Nano-indentation of hybrid silica coatings on surgical grade stainless steel. Thin Solid Films. 2008a;516:1082–7.

Ballarre J, López DA, Rosero NC, Durán A, Aparicio M, Ceré SM. Electrochemical evaluation of multilayer silica–metacrylate hybrid sol–gel coatings containing bioactive particles on surgical grade stainless steel. Surf Coat Technol. 2008b;203(1–2):80–6.

Ballarre J, Jimenez-Pique E, Anglada M, Pellice S, Cavalieri AL. Mechanical characterization of nano-reinforced silica based sol–gel hybrid coatings on AISI 316L stainless steel using nanoindentation techniques. Surf Coat Technol. 2009a;203(20):3325–31.

Ballarre J, López DA, Cavalieri AL. Frictional and adhesive behavior of organic–inorganic hybrid coatings on surgical grade stainless steel using nano-scratching technique. Wear. 2009b;266 (11–12):1165–70.

Ballarre J, Pellice SA, Schreiner WH, Ceré S. Coatings containing silica nanoparticles and glass ceramic particles applied onto surgical grade stainless steel. Key Eng Mater. 2009c;396–398:311–4.

Ballarre J, Manjubala I, Schreiner WH, Orellano JC, Fratzl P, Ceré S. Improving the osteointegration and bone-implant interface by incorporation of bioactive particles in sol–gel coatings of stainless steel implants. Acta Biomater. 2010;6(4):1601–9.

Ballarre J, Seltzer R, Mendoza E, Orellano JC, Mai YW, García C, Ceré SM. Morphologic and nanomechanical characterization of bone tissue growth around bioactive sol–gel coatings containing wollastonite particles applied on stainless steel implants. Mater Sci Eng C. 2011;31(3):545–52.

Ballarre J, Liu Y, Mendoza E, Schell H, Díaz F, Orellano JC, Fratzl P, García C, Ceré SM. Enhancing low cost stainless steel implants: bioactive silica-based sol–gel coatings with wollastonite particles. Int J Nano Biomater. 2012;4(1):33–53.

Ballarre J, Desimone PM, Chorro M, Baca M, Orellano JC, Ceré SM. Bone quality around bioactive silica-based coated stainless steel implants: analysis by Micro-Raman, XRF and XAS techniques. J Struct Biol. 2013;184(2):164–72.

Bi X, Patil CA, Lynch CC, Pharr GM, Mahadevan-Jansen A, Nyman JS. Raman and mechanical properties correlate at whole bone- and tissue-levels in a genetic mouse model. J Biomech. 2011;44(2):297–303.

Biehl V, Breme J. Metallic biomaterials. Mater Werkst. 2001;32:137–44.

Bohner M, Lemaitre J. Can bioactivity be tested in vitro with SBF solution? Biomaterials. 2009; 30(12):2175–9.

Brinker CJ, Scherer GW. Sol–gel science – the physics and chemistry of sol-gel processing. San Diego: Academic Press/Elsevier; 1990.

Cacciafesta P, Hallan KR, Watkinson AC, Allen GC, Miles JM, Jandt KD. Visualization of human plasma fibrinogen adsorbed on titanium implant surfaces with different roughness. Surf Sci. 2001;491:405–20.

Carden A, Morris MD. Application of vibrational spectroscopy to the study of mineralized tissues (Review). J Biomed Opt. 2000;5(3):259–68.

Carlisle EM. Silicon: a possible factor in bone calcification. Science. 1970;167(3916):279–80.
Cerruti M, Greenspan D, Powers K. Effect of pH and ionic strength on the reactivity of Bioglass® 45S5. Biomaterials. 2005;26(14):1665–74.
Chen Q, Thouas GA. Metallic implant biomaterials. Mater Sci Eng R Rep. 2015;87:1–57.
Chicot D, Lesage J. Absolute hardness of films and coatings. Thin Solid Films. 1995;254 (1–2):123–30.
Dao M, Chollacoop N, Van Vliet KJ, Venkatesh TA, Suresh S. Computational modeling of the forward and reverse problems in instrumented sharp indentation. Acta Mater. 2001;49 (19):3899–918.
de Damborenea JJ, Pellegri N, de Sanctis O, Duran A. Electrochemical behavior of SiO_2 sol–gel coatings on stainless steels. J Sol-Gel Sci Technol. 1995;4:239–44.
de Sanctis O, Gomez L, Pellegri N, Parodi C, Marajofsky A, Duran A. Protective glass coatings on metallic substrates. J Non Cryst Solids. 1990;121:338–43.
de Sanctis O, Gómez L, Pellegri N, Durán A. Behaviour in hot ammonia atmosphere of SiO_2-coated stainless steels produced by a sol–gel procedure. Surf Coat Technol. 1995;70(2–3):251–5.
Doorn PF, Campbell PA, Worrall J, Benya PD, MacKellop HA, Amstutz HC. Metal wear particle characterization from metal on metal total hip replacements: transmission electron microscopy study of periprosthetic and isolated particles. J Biomed Mater Res. 1998;42:103–11.
Duran A, Fernandez Navarro JM, Casariego P, Joglar A. Optical properties of glass coatings containing Fe and Co. J Non Cryst Solids. 1986;82(1–3):391–9.
Duran A, Conde A, Coedo AG, Dorado T, Garcia C, Cere S. sol–gel coatings for protection and bioactivation of metals used in orthopaedic devices. J Mater Chem. 2004;14(14):2282–90.
Fathi MH, Doostmohammadi A. Bioactive glass nanopowder and bioglass coating for biocompatibility improvement of metallic implant. J Mater Process Technol. 2009;209(3):1385–91.
Fischer-Cripps AC. Critical review of analysis and interpretation of nanoindentation test data. Surf Coat Technol. 2006;200:4153–65.
Fujikura K, Karpukhina N, Kasuga T, Brauer DS, Hill RG, Law RV. Influence of strontium substitution on structure and crystallisation of bioglass[registered sign] 45S5. J Mater Chem. 2012;22(15):7395–402.
Gallardo J, Galliano P, Duran A. Bioactive and protective sol–gel coatings on metals for orthopaedic prostheses. J Sol-Gel Sci Technol. 2001;21:65–74.
Galliano P, de Damborenea JJ, Pascual MJ, Duran A. sol–gel coatings on 316L stainless steel for clinical applications. J Sol-Gel Sci Technol. 1998;13:723–7.
Gamsjaeger S, Masic A, Roschger P, Kazanci M, Dunlop JWC, Klaushofer K, Paschalis EP, Fratzl P. Cortical bone composition and orientation as a function of animal and tissue age in mice by Raman spectroscopy. Bone. 2010;47(2):392–9.
Garcia C. Bioactivación de metales de uso ortopédico mediante recubrimientos producidos por sol-gel [PhD]. Madrid: Universidad Autonoma de Madrid- Fac. de Ciencias; 2004.
García C, Galliano P, Ceré S. Electrochemical evaluation of resistance to localised corrosion of vitreous coatings containing particles applied on metallic substrates for biomedical applications. Mater Lett. 2003;57:1810–4.
Garcia C, Ceré SM, Durán A. Bioactive coatings prepared by sol–gel on stainless steel 316L. J Non Cryst Solids. 2004;348:218–24.
García C, Durán A, Moreno R. Stability of suspensions of bioactive particles using hybrid organic–inorganic solutions as dispersing media. J Sol-Gel Sci Technol. 2005;34:1–7.
García C, Ceré S, Durán A. Bioactive coatings deposited on titanium alloys. J Non Cryst Solids. 2006;352(32–35):3488–95.
Gentleman E, Fredholm YC, Jell G, Lotfibakhshaiesh N, O'Donnell MD, Hill RG, Stevens MM. The effects of strontium-substituted bioactive glasses on osteoblasts and osteoclasts in vitro. Biomaterials. 2010;31(14):3949–56.
Goriainov V, Cook R, Latham JM, Dunlop DG, Oreffo ROC. Bone and metal: an orthopaedic perspective on osseointegration of metals. Acta Biomaterialia. 2014;10(10):4043–57.

Gorustovich AA, Steimetz T, Cabrini RL, Porto Lopez JM. Osteoconductivity of strontium-doped bioactive glass particles: a histomorphometric study in rats. J Biomed Mater Res A. 2010;92 (1):232–7.
Guglielmi M, Zenezini S. The thickness of sol gel silica coatings obtained by dipping. J Non Cryst Solids. 1990;121:303–9.
Hansen DC. Metal corrosion in the human body: the ultimate bio-corrosion scenario. Electrochem Soc Interface. 2008;17:31–4.
Harris AF, Beevers A. The effect of grit-blasting on surface properties for adhesion. Int J Adhes Adhes. 1999;19:445–52.
Hastings GW. Biomedical engineering and materials for orthopaedic implants. J Phys E Sci Instrum. 1980;13(6):599–607.
Helsen JA, Breme JH. Metals as biomaterials. Chichester: Wiley; 1998.
Hench LL, Ethridge EC. Biomaterials. An interfacial approach. Philadelphia: Academic; 1982. p. 384.
Hench LL, Paschall HA. Direct chemical bond of bioactive glass ceramic materials to bone and muscle. J Biomed Mater Res. 1973;7(3):25–42.
Hench LL, Wilson J. In: Hench LL, Wilson J, Hench LL, Wilson J, editors. An introduction to bioceramics, Advanced series in ceramics, vol. I. River Edge: World Scientific; 1993.
Huang L-Y, Zhao J-W, Xu K-W, Lu J. A new method for evaluating the scratch resistance of diamond-like carbon films by the nano-scratch technique. Diamond Relat Mater. 2002;11 (4):1454–9.
Innocenzi P, Guglielmi M, Gobbin M, Colombo P. Coating of metals by the sol gel dip-coating method. J Eur Ceram Soc. 1992;10:431–6.
Jacobs JJ, Silverton C, Hallab NJ, Skipor AK, Patterson L, Black J, Galante JO. Metal release and excretion from cementless titanium alloy total knee replacement. Clin Orthop Relat Res. 1999;358:173–80.
Jones JR. Review of bioactive glass: from Hench to hybrids. Acta Biomater. 2013;9(1):4457–86.
Jönsson B, Hogmark S. Hardness measurements of thin films. Thin Solid Films. 1984;114(3): 257–69.
Karimi A, Wang Y, Cselle T, Morstein M. Fracture mechanisms in nanoscale layered hard thin films. Thin Solid Films. 2002;420–421:275–80.
Kashyap BP, McTaggart K, Tangri K. Study on the substructure evolution and flow behaviour in type 316L stainless steel over the temperature range 21–900°C. Philos Mag. 1988;57(1): 97–114.
Kazanci M, Roschger P, Paschalis EP, Klaushofer K, Fratzl P. Bone osteonal tissues by Raman spectral mapping: orientation-composition. J Struct Biol. 2006;156(3):489–96.
Keding R, Rüssel C, Pascual MJ, Pascual L, Durán A. Corrosion mechanism of borosilicate sealing glasses in molten carbonates studied by impedance spectroscopy. J Electroanal Chem. 2002;528:184–9.
Kempf I, Semlitsch M. Massive wear of a steel ball head by ceramic fragments in the polyethylene acetabular cup after revision of a total hip prosthesis with fractured ceramic ball. Arch Orthop Trauma Surg. 1990;109:284–7.
Kheirkhah M, Fathi M, Salimijazi HR, Razavi M. Surface modification of stainless steel implants using nanostructured forsterite (Mg_2SiO_4) coating for biomaterial applications. Surf Coat Technol. 2015;276:580–6.
Kim Y-H, Kim J-S, Cho S-H. A comparison of polyethylene wear in hips with cobalt-chrome on zirconia heads. J Bone Joint Surg. 2001;83(B):742–50.
Kim HW, Koh YH, Kong YM, Kang JG, Kim HE. Strontium substituted calcium phosphate biphasic ceramics obtained by powder precipitation method. J Mater Sci Mater Med. 2004;15:1129–34.
King RB. Elastic analysis of some punch problems for a layered medium. Int J Solids Struct. 1987;23(12):1657–64.

Kokubo T, Kushitani H, Sakka S, Kitsugi T, Yamamuro T. Solutions able to produce in vivo surface – structure changes in bioactive glass – ceramic A. W. J Biomed Mater Res. 1990;24:721–34.

Kokubo T, Kushitani H, Ohtsuki C, Sakka S. Chemical reaction of bioactive glass and glass – ceramics with a simulated body fluid. J Mater Sci Mater Med. 1992;3:79–83.

Kokubo T, Kim H-M, Kawashita M. Novel bioactive materials with different mechanical properties. Biomaterials. 2003;24:2161–75.

Lasia A. Electrochemical impedance spectroscopy and its applications. In: Conway BE, Bockris J, White R, editors. Modern aspects of electrochemistry, vol. 32. New York: Kluwer/Plenum Publishers; 1999. p. 143–248.

Lesage J, Pertuz A, Chicot D. A new method to determine the hardness of thin films. Matéria. 2004;9(1):13–22.

Li P, De Groot K, Kokubo T. Bioactive $Ca_{10}(PO_4)6(OH)_2$-TiO_2 composite coating prepared by sol – gel process. J Sol–Gel Sci Technol. 1996;7:27–34.

Li X, Huang F, Curry M, Street SC, Weaver ML. Nanoscratch behaviour of dendrimer-mediated Ti thin films. Tribol Lett. 2005;19(4):273–80.

Li Y, Li Q, Zhu S, Luo E, Li J, Feng G, Liao Y, Hu J. The effect of strontium-substituted hydroxyapatite coating on implant fixation in ovariectomized rats. Biomaterials. 2010;31 (34):9006–14.

Liu X, Ding C. Morphology of apatite formed on surface of wollastonite coating soaked in simulate body fluid. Mater Lett. 2002;57(3):652–5.

Liu X, Ding C, Wang Z. Apatite formed on the surface of plasma-sprayed wollastonite coating immersed in simulated body fluid. Biomaterials. 2001;22(14):2007–12.

López DA, Duran A, Ceré S. Electrochemical characterization of AISI 316L stainless steel in contact with simulated body fluid under infection conditions. J Mater Sci Mater Med. 2008a;19 (5):2137–44.

López DA, Rosero-Navarro NC, Ballarre J, Durán A, Aparicio M, Ceré S. Multilayer silica-methacrylate hybrid coatings prepared by sol–gel on stainless steel 316L: electrochemical evaluation. Surf Coat Technol. 2008b;202(10):2194–201.

Lucas BN, Rosenmayer CT, Oliver WC. Mechanical characterization of sub-micron polytetrafluoroethylene (PTFE) thin films. Mater Res Soc Symp Proc. 1998;505:97–102.

Malzbender J, de With G, den Toonder JMJ. Elastic modulus, indentation pressure and fracture toughness of hybrid coatings on glass. Thin Solid Films. 2000;366(1–2):139–49.

Mammeri F, Le Bourhis E, Rozes L, Sanchez C. Elaboration and mechanical characterization of nanocomposites thin films part I: determination of the mechanical properties of thin films prepared by in situ polymerization of tetraethoxysilane in poly(methyl metacrylate). J Eur Ceram Soc. 2006;26:259–66.

Marie PJ. Strontium as therapy for osteoporosis. Curr Opin Pharmacol. 2005;5(6):633–6.

Martin JY, Schwartz Z, Hummert TW, Schraub DM, Simpson J, Lankford J. Effect of titanium surface roughness on proliferation, differentiation, and protein synthesis of human osteoblast – like cells (MG63). J Biomed Mater Res. 1995;29:389–401.

Matsko NB, Žnidaršič N, Letofsky-Papst I, Dittrich M, Grogger W, Štrus J, Hofer F. Silicon: the key element in early stages of biocalcification. J Struct Biol. 2011;174(1):180–6.

McGee MA, Howie DW, Costi K, Haynes DR, Wildenauer CI, Pearcy MJ, McLean JD. Implant retrieval studies of the wear and loosening of prosthetic joints: a review. Wear. 2000;241:158–65.

Mieszek A, Donesz-Sikorska A, Grzesiak J, Krzak J, Marycz K. Biological effects of sol–gel derived $ZrO_2$and SiO_2/ZrO_2 coatings on stainless steel surface – in vitro model using mesenchymal stem cells. J Biomater Appl. 2014;29(5):699–714.

Montemor MF, Cabral AM, Zheludkevich ML, Ferreira MGS. The corrosion resistance of hot dip galvanized steel pretreated with bis-functional silanes modified with microsilica. Surf Coat Technol. 2006;200(9):2875–85.

Nakonechna O, Cselle T, Morstein M, Karimi A. On the behaviour of indentation fracture in TiAlSiN thin films. Thin Solid Films. 2004;447–448:406–12.
Newman SD, Lotfibakhshaiesh N, O'Donnell M, Walboomers XF, Horwood N, Jansen JA, Amis AA, Cobb JP, Stevens MM. Enhanced osseous implant fixation with strontium-substituted bioactive glass coating. Tissue Eng Part A. 2014;20(13–14):1850–7.
Ni GX, Lu WW, Xu B, Chiu KY, Yang C, Li ZY, Lam WM, Luk KD. Interfacial behaviour of strontium-containing hydroxyapatite cement with cancellous and cortical bone. Biomaterials. 2006;27:5127–33.
Ni S, Chou L, Chang J. Preparation and characterization of forsterite (Mg_2SiO_4) bioceramics. Ceram Int. 2007;33(1):83–8.
Novak BM. Hybrid nanocomposite materials – between inorganic glasses and organic polymers. Adv Mater. 1993;5(6):422–33.
O'Donnell MD, Hill RG. Influence of strontium and the importance of glass chemistry and structure when designing bioactive glasses for bone regeneration. Acta Biomater. 2010;6(7):2382–5.
O'Donnell MD, Fredholm Y, de Rouffignac A, Hill RG. Structural analysis of a series of strontium-substituted apatites. Acta Biomater. 2008;4(5):1455–64.
O'Donnell MD, Candarlioglu PL, Miller CA, Gentleman E, Stevens MM. Materials characterisation and cytotoxic assessment of strontium-substituted bioactive glasses for bone regeneration. J Mater Chem. 2010;20(40):8934–41.
Okazaki Y, Gotoh E. Comparison of metal release from various metallic biomaterials in vitro. Biomaterials. 2005;26(1):11–21.
Oliver WC, Pharr GM. An improved technique for determining hardness and elastic modulus using load and displacement sensing indentation experiments. J Mater Res. 1992;7(6):1564–83.
Oliver WC, Pharr GM. Measurement of hardness and elastic modulus by instrumented indentation: advances in understanding and refinements to methodology. J Mater Res. 2004;19(1):3–20.
Omar S, Repp F, Desimone PM, Weinkamer R, Wagermaier W, Ceré S, Ballarre J. sol–gel hybrid coatings with strontium-doped 45S5 glass particles for enhancing the performance of stainless steel implants: electrochemical, bioactive and in vivo response. J Non Cryst Solids. 2015;425:1–10.
Panzavolta S, Torricelli P, Sturba L, Bracci B, Giardino R, Bigi A. Setting properties and in vitro bioactivity of strontium-enriched gelatin-calcium phosphate bone cements. J Biomed Mater Res A. 2007;84:965–72.
Park JB. Biomaterials science and engineering. New York: Premium Press; 1984.
Peitl O, Zanotto ED, Hench LL. High bioactive P_2O_5-Na_2O-CaO-SiO_2 glass – ceramic. J Non Cryst Solids. 2001;292:115–26.
Pellegri N, Sanctis O, Durán A. Preparation and microstructure study of borosilicate coatings produced by sol–gel. J Sol-Gel Sci Technol. 1994;2(1):519–23.
Pennington M, Grieve R, Sekhon JS, Gregg P, Black N, van der Meulen JH. Cemented, cementless, and hybrid prostheses for total hip replacement: cost effectiveness analysis. BMJ. 2013;346: f1026.
Peterson SL, McDonald A, Gourley PL, Sasaki DY. Poly(dimethylsiloxane) thin films as biocompatible coatings for microfluidic devices: cell culture and flow studies with glial cells. J Biomed Mater Res A. 2005;72(1):10–8.
Pourhashem S, Afshar A. Double layer bioglass-silica coatings on 316L stainless steel by sol–gel method. Ceram Int. 2014;40(1):993–1000.
Prikryl R, Cech V, Zajickova L, Vanek J, Behzadi S, Jones FR. Mechanical and optical properties of plasma-polymerized vinyltriethoxysilane. Surf Coat Technol. 2005;200(1–4):468–71.
Rothman RH, Cohn JC. Cemented versus cementless total hip arthroplasty: a critical review. Clin Orthop Relat Res. 1990;254:153–69.
Sahai N, Anseau M. Cyclic silicate active site and stereochemical match for apatite nucleation on pseudowollastonite bioceramic-bone interfaces. Biomaterials. 2005;26(29):5763–70.
Scharf TW, Barnard JA. Nanotribology of ultrathin a:SiC/SiC-N overcoats using a depth sensing nanoindentation multiple sliding technique. Thin Solid Films. 1997;308–309:340–4.

Semlitsch M, Willert HG. Clinical wear behaviour of ultra – high molecular weight polyethylene cups paired with metal and ceramic ball heads in comparison to metal – on – metal pairings of hip joint replacements. Proc Inst Mech Eng. 1997;211:73–88.

Simunkova S, Blahova O, Stepanek I. Mechanical properties of thin film-substrate systems. J Mater Process Technol. 2003;133(1–2):189–94.

Sneddon IN. The relation between load and penetration in the axisymmetric boussinesq problem for a punch of arbitrary profile. Int J Eng Sci. 1965;3(1):47–57.

Soloukhin VA, Posthumus W, Brokken-Zijp JCM, Loos J, de With G. Mechanical properties of silica-(meth)acrylate hybrid coatings on polycarbonate substrate. Polymer. 2002;43 (23):6169–81.

Soundrapandian C, Bharati S, Basu D, Datta S. Studies on novel bioactive glasses and bioactive glass–nano-HAp composites suitable for coating on metallic implants. Ceram Int. 2011;37 (3):759–69.

Steinemann SG. Metal implants and surface reactions. Injury. 1996;27 Suppl 3:SC16–22.

Strobel LA, Hild N, Mohn D, Stark WJ, Hoppe A, Gbureck U, Horch RE, Kneser U, Boccaccini AR. Novel strontium-doped bioactive glass nanoparticles enhance proliferation and osteogenic differentiation of human bone marrow stromal cells. J Nanopart Res. 2013;15(7):1–9.

Sun L, Berndt CC, Gross KA, Kucuk A. Material fundamentals and clinical performance of plasma-sprayed hydroxyapatite coatings: a review. J Biomed Mater Res. 2001;58(5):570–92.

Sychterz C, Engh CJ, Young A, Hopper RJ, Engh C. Comparison of in vivo wear between polyethylene liners articulating with ceramic and cobalt-chrome femoral heads. J Bone Joint Surg. 2000;82(B):948–51.

Webster TJ, Massa-Schlueter EA, Smith JL, Slamovich EB. Osteoblast response to hydroxyapatite doped with divalent and trivalent cations. Biomaterials. 2004;25(11):2111–21.

Wei G, Bhushan B, Jacobs SJ. Nanomechanical characterization of multilayered thin films structures for digital micromirror devices. Ultramicroscopy. 2004;100(3-4):375–89.

Willert HG, Buchhorn G. Particle disease due to wear of metal alloys. In: Biological, material and mechanical considerations of joint replacement. New York: Raven; 1993. p. 129–46.

Wolf B. Inference of mechanical properties from instrumented depth sensing indentation at tiny loads and indentation depths. Cryst Res Technol. 2000;35(4):377–99.

Wong CT, Chen QZ, Lu WW, Leong JC, Chan WK, Cheung KM, Luk KD. Ultrastructural study of mineralization of a strontium-containing hydroxyapatite (Sr-HA) cement in vivo. J Biomed Mater Res A. 2004;70:428–35.

Woodman JL, Black J, Nunamaker DM. Release of cobalt and nickel from a new total finger joint prosthesis made of vitallium. J Biomed Mater Res. 1983;17:8–655.

Xue W, Liu X, Zheng X, Ding C. In vivo evaluation of plasma-sprayed wollastonite coating. Biomaterials. 2005;26(17):3455–60.

Zhang Y, Mizuno M, Yanagisawa M, Takadama H. Bioactive behaviours of porous apatite- and wollastonite-containing glass-ceramic in two kinds of simulated body fluid. Mater Res Soc. 2003;18:433–41.